Noninvasive Functional Neuroimaging of Electrophysiological Brain Activities in Epilepsy Patients

A DISSERTATION
SUBMITTED TO THE FACULTY OF
UNIVERSITY OF MINNESOTA
BY

YUNFENG LU

IN PARTIAL FULFILLMENT OF THE REQUIREMENTS
FOR THE DEGREE OF
DOCTOR OF PHILOSOPHY

BIN HE, Advisor
Professor of Biomedical Engineering

May, 2014

Acknowledgements

I would like to express my most sincere appreciation to my advisor and mentor, Dr. Bin He, for his enormous guidance and support over the past six years. It is Dr. He's insightful advice and consistent assistance that help me make steady progress in research throughout the program.

I wish to thank my dissertation committee member Dr. Wei Chen, Dr. Emad Ebbini, and Dr. Matthew Johnson, for their time, support and valuable comments. I would like to thank our collaborator Dr. Gregory Worrell and his colleagues from Mayo Clinic, for the clinical data collection in adult epilepsy patients and for their expertise in the epilepsy research. I also would like to thank our collaborator Dr. Pongkiat Kankirawatana for the data collection of pediatric epilepsy patients.

I also wish to thank my lab colleagues at Biomedical Functional Imaging and Neuroengineering Laboratory at the University of Minnesota. Special thanks go to Dr. Lin Yang, Dr. Zhongming Liu, Dr. Christopher Wilke, Dr. Han Yuan, and Dr. Lei Ding, for sharing their knowledge and experience in functional neuroimaging and biomedical signal processing. I want to thank Mr. Abbas Sohrabpour for his help on the extent estimation work in Chapter 6. I would also like to thank Ms. Clara Huishi Zhang and Mr. Haojie Xu for the helpful discussion and the inspiring brainstorming. I am grateful for all other lab members Dr. Chengzong Han, Dr. Chenguang Liu, Dr. Gang Wang, Dr. Yakang Dai, Dr. Xu Li, Mr. Leo Mariappan, Dr. Xiaotong Zhang, Dr. Gang Hu, Ms. Zhaoye Zhou, Mr. Keith Jamison, Mr. Jiaen Liu, Ms. Kaitlin Cassady, Mr. Kai Yu, Mr. Long Yu, Mr. Abhrajeet Roy, Ms. Nessa Johnson, Mr. Bryan Baxter, and Mr. Brad Edelman.

To my beloved parents Huiwen Lu and Xiane Lu.

To my dear wife Panfang Hua.

Abstract

Epilepsy represents a chronic neurological disease that affects roughly 50 million people worldwide, and up to 30% of the patients do not respond effectively to medication. For those patients who experience frequent seizures and whose lives are greatly impacted, resective surgery removing epileptogenic foci is the last viable treatment option. The aim of this research is to develop and evaluate the EEG based noninvasive neuroimaging approaches to study the epileptogenic foci of epilepsy patients. Toward this goal, we have i) studied the feasibility of performing source connectivity based spatio-temporal dipole method for localizing ictal sources; ii) obtained the high-density scalp EEG recording in epilepsy patient and studied the effect of electrode numbers on source localization accuracy; iii) utilized the dynamic seizure imaging approach to track seizure activities in pediatric epilepsy patients; iv) established the high-frequency source imaging approach to image the scalp recorded pathological high-frequency activity in epilepsy patients; v) developed a method to estimate the source extent from noninvasive scalp recording. The methods were rigorously tested in a series of computer simulations and in different groups of epilepsy patients. Patient-specific structural MRI based head model was used to achieve high-accuracy volume conduction modeling of the brain source. Clinical diagnoses such as seizure onset zone of intracranial recording, surgical resection, and surgical outcome were used to evaluate the imaging approaches. The present study demonstrates the feasibility of utilizing high-density EEG recordings and high-resolution source imaging in localizing epileptic activity and indicates its potential application in pre-surgical planning of epilepsy patients.

Table of Contents

Chapter 1 Introduction

1.1 Motivation

The motivation of this dissertation is to develop noninvasive functional neuroimaging approaches to image the epileptic sources in order to help the pre-surgical planning of epilepsy treatment. Epilepsy represents a chronic neurological disease that affects roughly 50 million people worldwide. Epilepsy patients are often severely disabled by the unpredictable seizures that the disease manifests (Fisher et al., 2000, 2005). A panoply of pharmacological agents have been used for treating epilepsy. However, about 30% of patients do not respond effectively to currently available medication (Cascino, 1994). For those patients who experience frequent seizures and whose lives are greatly impacted, resective surgery that aims to remove epileptogenic foci remains one of the last viable treatment options (Palmini et al., 1991; Siegel et al., 2004; Engel, 2008). Yet, a successful surgical outcome can only be achieved if the epileptogenic foci are accurately and completely removed or disconnected. Accordingly, techniques that can accurately aid in localizing epileptogenic foci are of great importance for epilepsy surgery and a successful, seizure-free outcome.

Intracranial EEG has been used for detecting seizures (Ayala, et al., 2011; Tito et al., 2009, 2010) and delineating epileptogenic foci (Wilke et al., 2010). Intracranial EEG recording from ECoG grid or depth electrodes is also considered as the gold standard for identifying the seizure onset zone (Engel, 1987). Although intracranial recordings can provide direct neural-electrical measurement from the cortex, they are highly invasive, expensive, and painful for patients (Engel, 1987). Intracranial EEG also has limited

cortical coverage due to the restriction of surgical operation. Heretofore, noninvasive positron emission tomography (PET) and ictal subtraction single photon emission computed tomography (SPECT) have been utilized to extract metabolic and perfusion information from epilepsy patients (Van Paesschen et al., 2007). FMRI, yet another functional imaging technique, has been used to detect hemodynamic responses from the neural activities of epilepsy patients (Gotman, 2008; Vulliemoz et al., 2010; Moeller et al., 2011; You et al., 2011). Attempts have been made in order to image (and thus localize) epileptic foci from noninvasive measurements (Ebersole, 2000; Oishi et al., 2002; Plummer et al., 2008; Brodbeck et al., 2009). Previous studies have, in fact, demonstrated that EEG source imaging could be a useful tool for localizing epileptogenic zones because of its high temporal resolution at the millisecond scale as well as its noninvasive nature. However, EEG has a limited spatial resolution due to the smearing effect of the head volume conduction and the conductivity heterogeneity (Lai et al., 2005; Zhang et al., 2006). In order to image epileptogenic zones for aiding pre-surgical planning, there is a need to enhance the spatial resolution of EEG.

Scalp EEG has been widely used in clinical settings to characterize seizure activities in epilepsy patients. Patients typically undergo long-term video monitoring to capture their seizures and to help lateralize or localize seizure onset regions. Recent advancement in the EEG source imaging technique has made it possible to study the activities in the brain source space in addition to the traditional scalp EEG trace inspection. Many studies have shown the capability of EEG source imaging in localizing the brain sources in interictal epileptiform discharges (He et al., 1987; Ebersole, 2000;

Lantz et al., 2003; Zhang et al., 2003; Michel et al., 2004; Gavaret et al., 2004; Sperli et al., 2006; Plummer et al., 2008; Brodbeck et al., 2010; Wang et al., 2010; Lai et al., 2011). The imaging of seizure activities and other epileptic activities still remains a challenge due to the various types of ictal patterns and contamination of moving artifacts in EEG (Assaf and Ebersole, 1997; Worrell et al., 2000; Lantz et al., 2001; Ding et al., 2007; Koessler et al., 2010; Yang et al., 2011).

1.2 The organization of this thesis

This thesis covers some of the research outcomes we achieved regarding the noninvasive functional neuroimaging of epileptic sources from scalp EEG.

Chapter 2 gives the background introduction to the EEG and the EEG source imaging principles. Chapter 3 introduces the source space functional connectivity analysis for localizing the seizure sources from high-density scalp EEG. The effect of electrode numbers was also quantitatively evaluated with a series of computer simulations and patient data analysis. Chapter 4 reports a study of utilizing the dynamic seizure imaging approach for imaging the seizure activity in pediatric epilepsy patients. Chapter 5 presents a study of imaging the high-frequency brain activity in epilepsy patients. A paradigm aiming at investigating the underlying sources of scalp recorded high-frequency activity was proposed in the study. Chapter 6 covers the study of imaging source extent from noninvasive EEG recording. Chapter 7 concludes the work of this thesis and discusses the limitations and the future works.

Chapter 2 Basics of EEG

2.1 Introduction to EEG

Electroencephalography (EEG) is the noninvasive recording of synchronized neuronal activity over the scalp. EEG together with magnetoencephalography (MEG) is so far the only noninvasive recording of the neurophysiological activity of the brain. EEG has the advantage of high temporal resolution and the EEG recording can capture the neurophysiological data at the millisecond time scale. Thus, EEG has been widely used to study the normal brain function in healthy subjects and the pathological brain functional in diseased brain (Michel et al., 2004; He et al., 2011). Scalp EEG is used in clinical settings to characterize seizure activities in epilepsy patients. Epilepsy patients will typically undergo long-term video monitoring to capture their seizures and to help lateralize or localize seizure onset regions.

2.2 EEG forward modeling

EEG has a high temporal resolution capturing the fine brain dynamics. However, the spatial resolution of EEG is somehow limited due to the smearing effect of volume conduction of the head, especially for the low conductive skull layer. It is thus very important to solve the inverse problem to have a precise estimation of the EEG sources. Forward modeling including the source modeling and volume conduction modeling is the prerequisite of solving the inverse solutions. Forward modeling is used to establish the connections between the source activity of brain and EEG potential measurement over scalp.

The scalp EEG can be represented by modeling the brain electrical sources and the volume conduction effects. The general problem can be written in Equation (2.1).

$$\Phi = A(R,Q)\,S \tag{2.1}$$

The Nm-by-Nt matrix Φ is the electrical potential measured on the scalp, the Nm-by-3Ns matrix $A(R,Q)$ is the transfer matrix (or lead-field matrix), the Ns-by-1 vector R is the location of sources, the Ns-by-3 matrix Q is the orientation of sources, and the Ns-by-3Nt matrix S is the activity of brain sources. Nm is the number of EEG measurement on the scalp, Nt is the number of recorded samples in EEG, and Ns is the dimension of EEG source locations in source domain.

2.2.1 Source modeling

An important issue in EEG source imaging is modeling source configurations. Dipolar source model and distributed source model are the most commonly used source models in EEG source imaging (He et al, 2002; Michel et al., 2004).

The assumption for dipolar source model is that a few discrete sources are adequate to explain the scalp potential. Studies have shown that equivalent current dipolar source model can be successfully applied in localizing focal epileptiform activities (Assaf and Ebersole, 1997; Gavarat et al., 2004). However, *a priori* knowledge of the source number is usually hard to determine and dipolar models cannot adequately represent the extent of the sources, despite efforts on estimation of the number of dipoles (Bai and He, 2005, 2006). In distributed source model, current sources are located in the whole source space such as 3D brain volume or 2D cortical surface. Various inverse methods were successfully employed to image the electrical sources of epilepsy patients

from dipolar source model and distributed source model (Assaf and Ebersole, 1997; Gavarat et al., 2004; Michel et al., 2004; Holmes, 2008). To utilize EEG source analysis as a pre-surgical evaluation tool in clinical procedure, more studies are needed to investigate the feasibility of source modeling in localizing epileptogenic foci of epilepsy patients.

2.2.2 Volume conduction modeling

The EEG measurement over the scalp can be modeled as the electrical potential generated by the current source through the brain volume conduction. If the homogeneous assumption was made for the conducting volume, the relationship between the electrical potential and current density can be modeled as

$$4\pi\sigma\Phi = \int_v \bar{J}^i \cdot \nabla\left(\frac{1}{r}\right) dv \tag{2.2}$$

where σ is the conductivity value of the volume, Φ is the potential measurement, $\bar{J}$ is the current density, r is the location of the potential sensor related to location of the current density. When the volume conduction is modeled as surrounded by a few layers with different conductivity values, the relationship between potential and current source can be modeled as

$$4\pi\sigma\Phi(r) = \int_v \bar{J}^i \cdot \nabla\left(\frac{1}{r}\right) dv + \sum_j \int_{s_j} (\sigma_j'' - \sigma_j')\Phi \nabla\left(\frac{1}{r}\right) \cdot d\bar{S}_j \tag{2.3}$$

where S_j is the boundary between two conductive layers with conductivity values equal to σ'' and σ'.

EEG source imaging techniques can noninvasively study brain activities by modeling the brain sources and volume conductor (He et al., 1987; Michel et al., 2004;

Plummer et al., 2008; He et al., 2011). In the study, a patient-specific boundary element method (BEM) head model was obtained from individual MRI and used for EEG source analysis to improve the spatial resolution. Studies have shown that more precise source localization results can be obtained in realistic-geometric head models compared to simple spherical head models (Herrendorf et al., 2000; Wang et al., 2010).

Structural MRI T1 images (voxel size: 0.9375* 0.9375* 1.0 mm^3, 166 slices on average) can be obtained for each patient from either a 1.5 Tesla or 3 Tesla GE Signa scanner (General Electric Medical Systems, Milwaukee, WI). These MRI images can be used to build realistic geometry BEM of the head, which consists of three layers: scalp, skull and brain. The patient specific BEM can be constructed from the segmentation results of the three layers using CURRY6 software (Compumedics, Charlotte, NC). The conductivity values of scalp, skull and brain can be set as 0.33 S/m, 0.0165 S/m and 0.33 S/m, respectively (Oostendorp et al., 2000; Lai et al., 2005).

The performance of EEG source imaging could further be improved by incorporating more *a prior* information such as anisotropic conductivities (Michel et al., 2004) and fMRI constrains (He & Liu, 2008; Liu and He, 2008; Yang et al., 2010) of the patients. Future studies in more sophisticated finite element method (FEM) head models may be necessary to further improve the application of EEG source imaging in epilepsy patients.

2.3 EEG inverse solutions

Recent advancement in the EEG source imaging technique has made it possible to study the activities in the brain source space in addition to the traditional scalp EEG trace inspection. Many studies have shown the capability of EEG source imaging in localizing

the brain sources in interictal epileptiform discharges (He et al., 1987; Ebersole, 2000; Lantz et al., 2003; Zhang et al., 2003; Michel et al., 2004; Gavaret et al., 2004; Sperli et al., 2006; Plummer et al., 2008; Brodbeck et al., 2010; Wang et al., 2010; Lai et al., 2011).

The inversion problem can be solved by getting the solutions for the following general optimization problem.

$$\arg\min_{S} \left(\left\| \Phi - A * S \right\|_2 + \left\| \lambda * B * S \right\|_2 \right) \tag{2.4}$$

where $\left\| \bullet \right\|_2$ is the Frobenius norm operator (L2 norm), λ is the regularization term, and B is the source weighting matrix for the inverse solution. Varieties of source models and source imaging methods can be applied to solve the above inverse problem. For instance, if B is the identify matrix, the solution is the regular minimum norm estimation (MNE). The solution is low resolution brain electromagnetic tomography (LORETA) when the Laplacian matrix was used to solve the problem. However, the source imaging results from L2-norm type methods are generally over-smoothed.

By performing the sparse L1 norm on the inverse problem, we can obtain some spare source of the EEG activity. Furthermore, if we apply the sparse L1 norm on the spatial gradient of the source, we are able to reconstruct the signal that only has limited spatial jump, i.e. the edges of the source distribution. The new optimization problem becomes following

$$\arg\min_{s} \left(\left\| \Phi - A * S \right\|_2 + \left\| \lambda * V * S \right\|_1 \right) \tag{2.5}$$

where $\left\| \bullet \right\|_1$ is the L1 norm for spare solution, V is the discrete gradient operator. The reason for using L1 norm in (2.5) is that using L0 norm, which is basically counting the non-zero elements of a vector, would make the problem non-convex and difficult to solve. However, it is well-known that interchanging L0 norm with L1 norm will give solutions that are close to the desired solutions (Donoho, 2004). As the optimization problem formulated in (2.5) is a convex optimization problem, solving (2.5) is easy due to the abundance of developed techniques in convex optimization. Thus, solving such seemingly complex optimization problem will not be a difficulty.

Cortical potential imaging techniques was also applied in epilepsy patients and found the consistency between epileptic cortical areas and surgical resections (Zhang et al., 2003; Lai et al., 2011). Good performance of equivalent current dipole modeling was demonstrated in source analysis of temporal and frontal lobe epilepsy (Gavaret et al., 2004, 2006). Parameterization of ictal data in time domain or frequency domain was also applied to study ictal source analysis (Worrell et al., 2000; Morlet and Gotman, 2001; Lantz et al., 2001; Boon et al., 2002).

Chapter 3 Source Space Connectivity Analysis in Epilepsy Patients

3.1 Introduction

Epilepsy represents a chronic neurological disease that affects roughly 50 million people worldwide. Epilepsy patients are often severely disabled by the unpredictable seizures that the disease manifests (Fisher et al., 2000, 2005). A panoply of pharmacological agents have been used for treating epilepsy. However, about 30% of patients do not respond effectively to currently available medication (Cascino, 1994). For those patients who experience frequent seizures and whose lives are greatly impacted, resective surgery that aims to remove epileptogenic foci remains one of the last viable treatment options (Palmini et al., 1991; Siegel et al., 2004; Engel, 2008). Yet, a successful surgical outcome can only be achieved if the epileptogenic foci are accurately and completely removed or disconnected. Accordingly, techniques that can accurately aid in localizing epileptogenic foci are of great importance for epilepsy surgery and a successful, seizure-free outcome.

Intracranial EEG has been used for detecting seizures (Ayala, et al., 2011; Tito et al., 2009, 2010) and delineating epileptogenic foci (Wilke et al., 2010). Intracranial EEG recording from ECoG grid or depth electrodes is also considered as the gold standard for identifying the seizure onset zone (Engel, 1987). Although intracranial recordings can provide direct neural-electrical measurement from the cortex, they are highly invasive, expensive, and painful for patients (Engel, 1987). Intracranial EEG also has limited cortical coverage due to the restriction of surgical operation. Heretofore, noninvasive

positron emission tomography (PET) and ictal subtraction single photon emission computed tomography (SPECT) have been utilized to extract metabolic and perfusion information from epilepsy patients (Van Paesschen et al., 2007). FMRI, yet another functional imaging technique, has been used to detect hemodynamic responses from the neural activities of epilepsy patients (Gotman, 2008; Vulliemoz et al., 2010; Moeller et al., 2011; You et al., 2011). Attempts have been made in order to image (and thus localize) epileptic foci from noninvasive measurements (Ebersole, 2000; Oishi et al., 2002; Plummer et al., 2008; Brodbeck et al., 2009). Previous studies have, in fact, demonstrated that EEG source imaging could be a useful tool for localizing epileptogenic zones because of its high temporal resolution at the millisecond scale as well as its noninvasive nature. However, EEG has a limited spatial resolution due to the smearing effect of the head volume conduction and the conductivity heterogeneity (Lai et al., 2005; Zhang et al., 2006). In order to image epileptogenic zones for aiding pre-surgical planning, there is a need to enhance the spatial resolution of EEG.

Many efforts have been devoted to studying noninvasive EEG source imaging approaches in medically intractable epilepsy patients. Studies have shown that electrical source imaging can be a useful tool in identifying epileptogenic foci in patients with normal or lesion-evident MRI results (Brodbeck et al., 2009, 2010). In a few studies, significant correlations were reported between estimated neural-electrical sources and surgical resections (Michel et al., 2004; Lai et al., 2011). Moreover, some investigators have combined EEG and functional MRI for these purposes (Gotman et al., 2006; Vulliemoz et al., 2011). However, source imaging performed with this technique relied

mainly on interictal spikes. Considering the clinical importance of ictal events in lateralizing or localizing seizure onset zone, source analysis based on ictal activities remains to be studied (Assaf and Ebersole, 1997; Worrell et al, 2000). The spatial-temporal source localization approach (FINE) was previously developed and studied in systematic computer simulations and motor evoked potential experiments (Xu et al., 2004; Ding and He, 2006). It was also applied to image epileptic sources in patients with lesion-evident MRI studies (Ding et al., 2007). Additional studies have suggested that more accurate source imaging results could be obtained by increasing the number of scalp EEG signal channels (Lantz et al., 2003; Michel et al., 2004; Holmes et al., 2008).

The aim of this study is to investigate a high resolution electrical source imaging technique and high-density EEG recordings for the purpose of identifying seizure onset zones in patients with medically intractable partial epilepsy. We applied a patient-specific boundary element method (BEM) head model and the source localization approach to obtain high spatial-temporal resolution of sources that corresponded to scalp ictal activities. Functional connectivity analysis was then utilized to identify the primary ictal source from propagated sources (Lu et al., 2012a). Further, we investigated the localization improvement that can be achieved using dense array EEG recording. Five configurations with 76, 64, 48, 32, and 21 electrodes were tested. The localization of seizure onset zone was performed for each configuration using downsampled data. Computer simulations were also conducted to study the effect of electrode numbers in EEG source imaging. The computer simulation results were compared with the simulated

sources and the patient data analysis results were evaluated with surgical resections in these patients.

3.2 Methods

3.2.1 Patients and data acquisition

Ten patients with medically intractable partial epilepsy were studied using a protocol approved by the Institutional Review Boards of the University of Minnesota and Mayo Clinic. The patients are consecutive partial epilepsy patients selected according to the following criteria: (1) seizures were captured in the high-density EEG recording, (2) the patients underwent surgical resections after pre-surgical workup, (3) the patients were seizure free after the resective surgery, (4) high-resolution structural MRI were acquired before and after their surgical operation. The surgical resections were used to evaluate the performance of source imaging results, and this information was not used in the source analysis. All the patients had presurgical evaluation including high-resolution structural MRI, long-term video-EEG monitoring (5.6 days on average) using 76 channels at Mayo Clinic (Rochester, MN, USA). All the patients underwent surgery to remove epileptogenic zones, and were rendered seizure free after one year follow up of the surgical operation by skilled epileptologists. Table 3.1 summarized the patients' characteristics.

Table 3.1 Clinical information of the patients in this study.

Patient	Gender	Age	Ictal symptoms	Pathology	MRI lesion	Depth electrode/Surgery	Outcome
1	Male	32	Behavioral arrest, oral automatisms, and right arm posturing	Left hippocampus: mesial temporal sclerosis	Left HC atrophy and T2 signal	Left anterior temporal lobectomy	ILAE-1
2	Female	50	Sense of impending doom, oral automatisms	Right hippocampus: mesial temporal sclerosis	Right HC atrophy	Right temporal lobectomy	ILAE-1
3	Female	22	Left hand nose wiping, and oral automatisms	Subcortical and subpial gliosis	Left frontal polar encephalomalcia	Left frontal cortectomy	ILAE-1
4	Male	58	Swallowing and oral automatisms; non-forced head turning to left	Right temporal subpial gliosis	Normal	Right temporal depth electrode/Right anterior temporal lobectomy	ILAE-1
5	Female	28	Right hand automatisms, oral automatisms, ictal scream, and hypermotor activity	Gliosis, subpia, subcortical, entorhinal cortex	Normal	Left temporal depth electrode/Left temporal lobectomy	ILAE-1
6	Female	45	Behavioral arrest, oral automatisms, and right arm posturing	Severe subpial gliosis consistent with chronic seizure disorder	Mild generalized cerebellar atrophy	Right temporal lobectomy	ILAE-2
7	Male	49	Behavior arrest followed by oral automatisms	Cortex and white matter with non-specific mild gliosis	Focal mass anterior left temporal lobe	Left temporal lobectomy	ILAE-1
8	Female	33	Behavioral arrest, staring, chewing type oral automatisms	Right hippocampus: mesial temporal sclerosis	Bilateral increased T2 signal in HC without evidence of atrophy	Right temporal lobectomy	ILAE-1
9	Female	25	Oral automatisms and right hand more often than left hand automatisms	Right hippocampus: mesial temporal sclerosis	Normal	Right temporal lobectomy	ILAE-1
10	Female	51	Lip smacking movements, tightness of the left face, head turn to the left	Gliosis, subpia, subcortical, entorhinal cortex	T2 hyperintensity in the right inferior temporal	Right anterior temporal lobectomy	ILAE-1

ILAE: International league against epilepsy. ILAE-1: Completely seizure free; no auras. ILAE-2: Only aura, no other seizures.

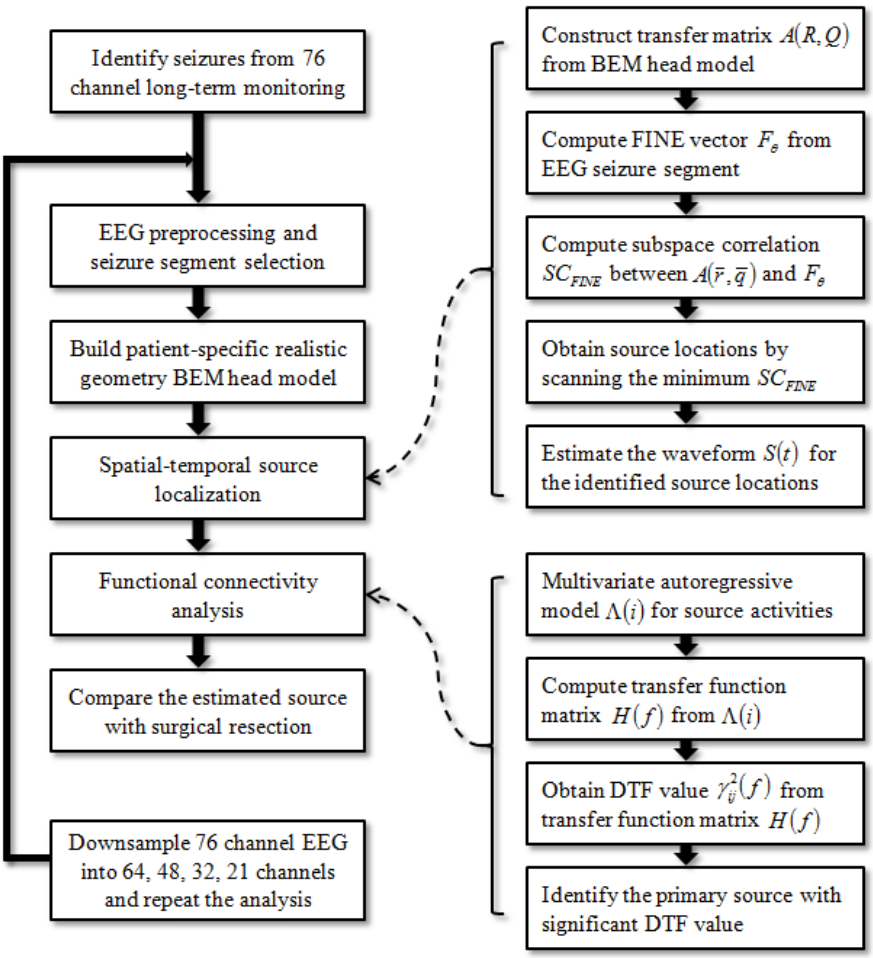

Fig. 3.1 Diagram of procedural steps in the present seizure source imaging.

During the long-term monitoring, scalp EEG was recorded from 76 electrodes according to the modified international 10-20 system, with 500 Hz sampling frequency and 1-70 Hz band-pass filtering. Standard electrode locations were utilized for the source analysis. The long-term video EEG was reviewed for seizure activities and seizure onset time was marked by experienced epileptologists. Band-pass filter of 1 and 30 Hz was used to reduce the high frequency noise and DC linear trend of EEG. Among the captured seizures (1-4 seizures per patient, 27 seizures in total) from the patients, the ictal data in 4

seizures were excluded due to the large moving artifacts and all the other seizures (23 seizures) were used in the study. Seizure segments with approximately 2-3 s were selected after seizure onset time. The quasi-stationary and artifact-free conditions of the selected segment can be examined by inspecting the waveforms and time-frequency representation (TFR) of the EEG signals. Fig. 3.2 shows the waveform and TFR of the 76-channel EEG signals in one seizure.

Structural MRI T1 images (voxel size: 0.9375* 0.9375* 1.0 mm^3, 166 slices on average) were obtained for each patient from a 1.5 Tesla or 3 Tesla GE Signa scanner (General Electric Medical Systems, Milwaukee, WI). These MRI images were used to build realistic geometry BEM of the head, which consists of three layers: scalp, skull and brain. The patient specific BEM was constructed from the segmentation results of the three layers using CURRY6 software (Compumedics, Charlotte, NC). The conductivity values of scalp, skull and brain were set as 0.33 S/m, 0.0165 S/m and 0.33 S/m, respectively (Oostendorp et al., 2000; Lai et al., 2005).

3.2.2 Electrical source imaging

The spatial-temporal source localization approach (FINE) was previously studied in both computer simulations and human subjects (Xu et al., 2004; Ding and He, 2006; Ding et al., 2007). The problem can be expressed as

$$\Phi(t) = A(R,Q)S(t) \tag{3.1}$$

where $\Phi(t)$ is the electrical potential measurement on the scalp at time t, $A(R,Q)$ is the transfer matrix from source locations R with source orientations Q, $S(t)$ is the source activity at time t. The equation is meant to find the source locations R and source

orientations Q in three dimensional source spaces that best fit the signal subspace. Once the transfer matrix $A(R,Q)$ is determined, the source waveforms $S(t)$ can be estimated by solving the inverse problem.

Patient-specific realistic geometry BEM head models with three layers (scalp, skull, brain) were built from the structural MRI images. The lead field matrix $A(R,Q)$ was then computed from the BEM head model (He et al., 1987; Hämäläinen and Sarvas, 1989). We employed the equivalent current dipole as the source model, and the source space was set as the whole three dimensional brain. The subspace correlation (SC) between the source dipolar topographies and noise-only scalp EEG subspace were defined as

$$SC_{FINE}(r) = \min_{\bar{q}} \left(\frac{A(\bar{r},\bar{q})^T F_\theta F_\theta A(\bar{r},\bar{q})}{A(\bar{r},\bar{q})^T A(\bar{r},\bar{q})} \right) \tag{3.2}$$

where $\bar{r}$ is the possible source location at three dimensional source space, $SC_{FINE}(r)$ is the source correlation value at location $\bar{r}$, $A(\bar{r},\bar{q})$ is the transfer matrix at source location $\bar{r}$ with source orientation $\bar{q}$, F_θ is the FINE vector projected to the noise subspace. The sources are obtained by scanning the locations with local minimum of subspace correlation. Subspace correlation threshold is set at 5% and only subspace correlation values below it are considered as possible sources. Source waveforms of the identified sources are then estimated by solving the overdetermined inverse problem.

3.2.3 Functional connectivity analysis

The functional connectivity analysis utilizing DTF (Kaminski and Blinowska, 1991; Kaminski et al., 2001) is an extension of Granger causality theory (Granger, 1969). Instead of being only suitable for paired-wise directional causality as in Granger theory,

the DTF can be applied to analyze connectivity among multi-channel signals (Astolfi et al., 2004, 2005; Babiloni et al., 2005; Wilke et al., 2009, 2010; He et al., 2011). Multivariate autoregressive (MVAR) modeling was firstly applied to estimate the model parameters of signals as

$$X(t) = \sum_{i=1}^{p} \Lambda(i) X(t-i) + E(t) \tag{3.3}$$

where $X(t)$ is the signal data at time t, $\Lambda(i)$ are the matrices of multivariate model coefficients, p is the model order, and $E(t)$ is a vector of multivariate white noise. After transforming MVAR model parameters into frequency domain,

$$\Lambda(f) X(f) = E(f) \tag{3.4}$$

$$X(f) = \Lambda^{-1}(f) E(f) = H(f) E(f) \tag{3.5}$$

where $\Lambda(f) = \sum_{k=1}^{p} \Lambda_k e^{-j2\pi f \Delta t k}$, and $H(f)$ is the transfer function matrix of the system. The DTF value $\gamma_{ij}^2(f)$ from signal j to signal i can be obtained by normalizing the system transfer function matrix

$$\gamma_{ij}^2(f) = \frac{\left|H_{ij}(f)\right|^2}{\sum_{m=1}^{n} \left|H_{im}(f)\right|^2} \tag{3.6}$$

Signals which have significant directional DTF value to other signals were considered to have directional causality to other signals. Nonparametric surrogate testing was conducted to test the significance. The shuffling procedure destroying the phase information of the original signals was repeated 5000 times and the DTF values with the significance level $p<0.05$ were considered as directional significant. Spatial-temporal

localized sources having significant directional DTF values to other sources were considered as the primary sources.

3.2.4 Evaluation of source imaging results

The source imaging results were evaluated with the surgically resected areas of the patients. Structural MRI images were acquired from these patients a few months after their surgical operation (General Electric Medical Systems, Milwaukee, WI). The surgically resected areas were evidenced by post-operative magnetic resonance studies. Since all the patients were seizure free after the surgical operation following one year follow-up, the resected areas of the patients were used as our reference to validate the EEG source imaging results. More specifically, localization error of clinical data, which was defined as the distance between the estimated source to the boundary of surgical resection, was applied to evaluate the source imaging results in patients. The localization error was considered zero if the estimated source was located inside the surgical resection.

3.2.5 Effect of high-density EEG for source imaging

Computer simulation of ictal source analysis was performed using configurations of different electrode numbers and noise levels. Dipolar sources with random location and orientation were simulated in the 3D brain, and the time course of the source was generated from a damped sinusoidal waveform. A realistic geometric BEM head model was utilized to compute lead-field matrix and simulate 76-channel scalp EEG. Gaussian white noise with different signal-to-noise ratios (SNRs) was added to the generated scalp EEG. The simulated 76-channel EEG was spatially downsampled into uniformly

distributed 64, 48, 32, and 21 electrode configurations. At each electrode setting and noise level, FINE was applied to estimate the sources in the 3D brain. Localization error of computer simulation, which was defined as the distance between estimated source and truly simulated source, was incorporated to quantitatively compare the performance of source imaging with different numbers of electrodes.

We then tested the effect of electrode numbers on EEG source imaging results in patient data. As in computer simulation, patient EEG with different electrode configurations (76, 64, 48, 32, and 21 electrodes) was used for ictal source analysis. The sources were localized using the same procedure for all electrode configurations. Localization error of clinical data represents the distance between the estimated source to the boundary of surgical resection. Statistical analysis was performed to test the significance between low density configurations and high density configurations. Dependent t-test was applied to test the significant paired difference between any two electrode configurations. One-way analysis of variance (ANOVA) was also used to test the significant group difference among all the electrode configurations.

3.3 Results

Ten patients with medically intractable epilepsy were analyzed in this study. High-density EEG was recorded in these patients during the long-term video monitoring at Mayo Clinic. All of the patients had resective surgery and were seizure-free after one-year follow up of the operation.

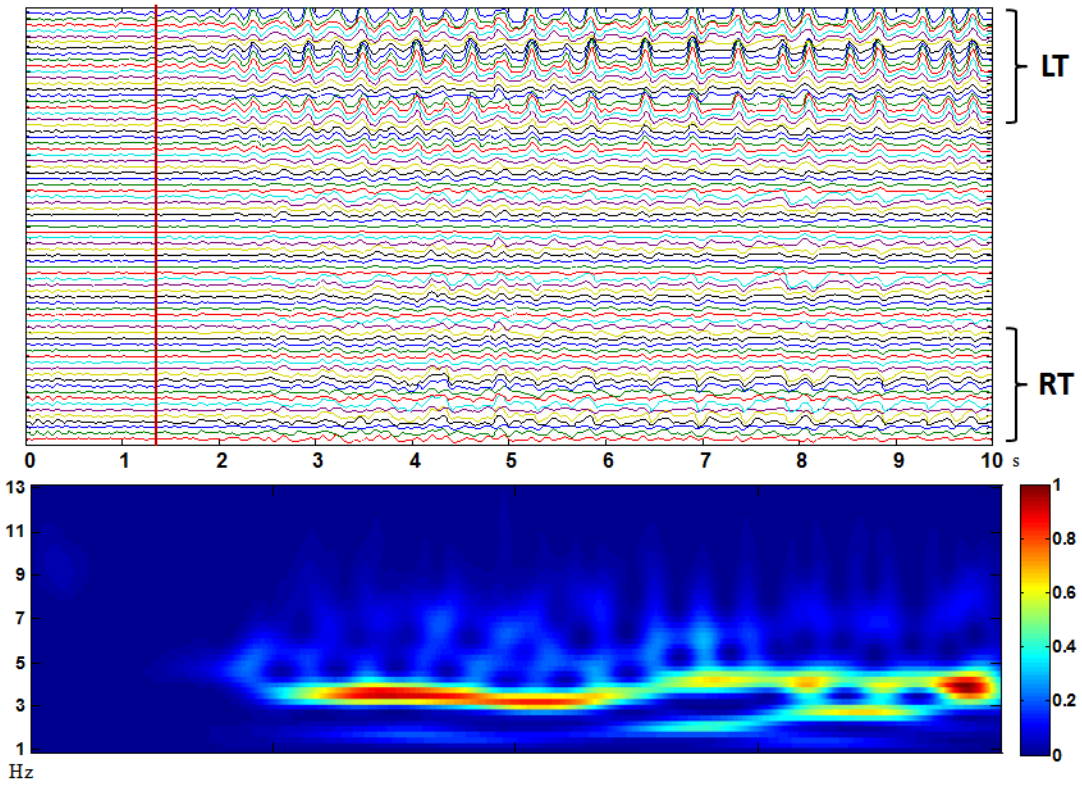

Fig. 3.2 The waveform and time-frequency representation of the ictal scalp EEG data with 76-channel recordings. The red vertical line marked on the EEG waveform is the seizure onset time recognized by experienced epileptologists. EEG channels near left temporal lobe (LT) and right temporal lobe (RT) of the patient were marked on the right side of the EEG waveform.

Patient 1 was a 32-year-old male epilepsy patient suffering from left temporal lobe seizures. Four seizures were captured from this patient during the pre-operative long-term video EEG recording. The scalp EEG waveform (Fig. 3.2) of one seizure in this patient showed rhythmic delta activities that were initially observed in left temporal electrodes and then remained prominently during the rest of the ictal period. The rising of such rhythmic activities were also found in right temporal electrodes, but in a temporally delayed and attenuated manner.

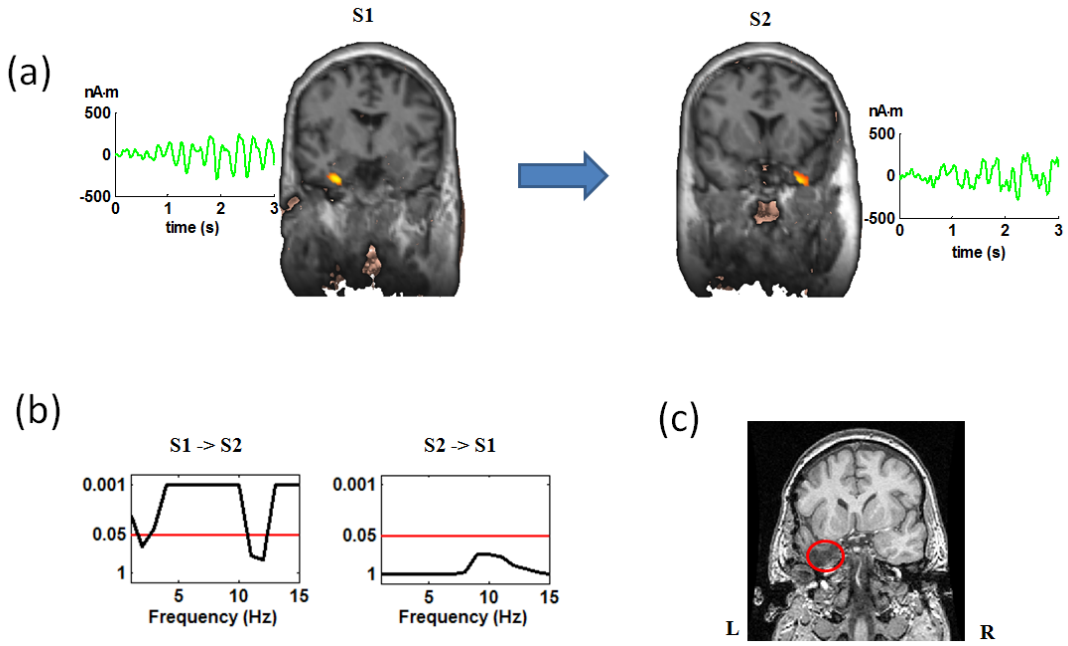

Fig. 3.3 Source imaging results of Patient 1. (a) Waveforms (green curves), locations (highlights on grey MRI images), and directional causality (blue arrow) of two sources (S1, S2). (b) Significance level of directional DTF values between S1 and S2. Statistical DTF value above the red line is significant with p-value < 0.05. (c) Surgical resection marked by red circle on post-operative MR image. Patient 1 had left temporal lobe epilepsy.

The source imaging results for Patient 1 is shown in Fig. 3.3. Two sources (S1, S2) are identified after applying FINE. Fig. 3.3a, the source locations and extent are superimposed and displayed with the pre-operative structural MRI of the patient. The waveforms of the two sources are also displayed next to the sources in Fig. 3.3a. The arrow between the sources indicates the connectivity analysis results, directing from primary source to propagated source. Fig. 3.3b shows the significance level of DTF information flow between S1 and S2 as a function of frequency. DTF results above the red line indicate the significant information flow ($p < 0.05$) from this source to the other source. In this patient, S1 had significant information flow to S2 while no such

significance can be observed from S2 to S1. S1 was thus identified as the primary source, which is located in the left temporal lobe. Fig. 3.3c shows the post-operative MR image with red circle marking out the surgically resected area that is located in the left temporal lobe.

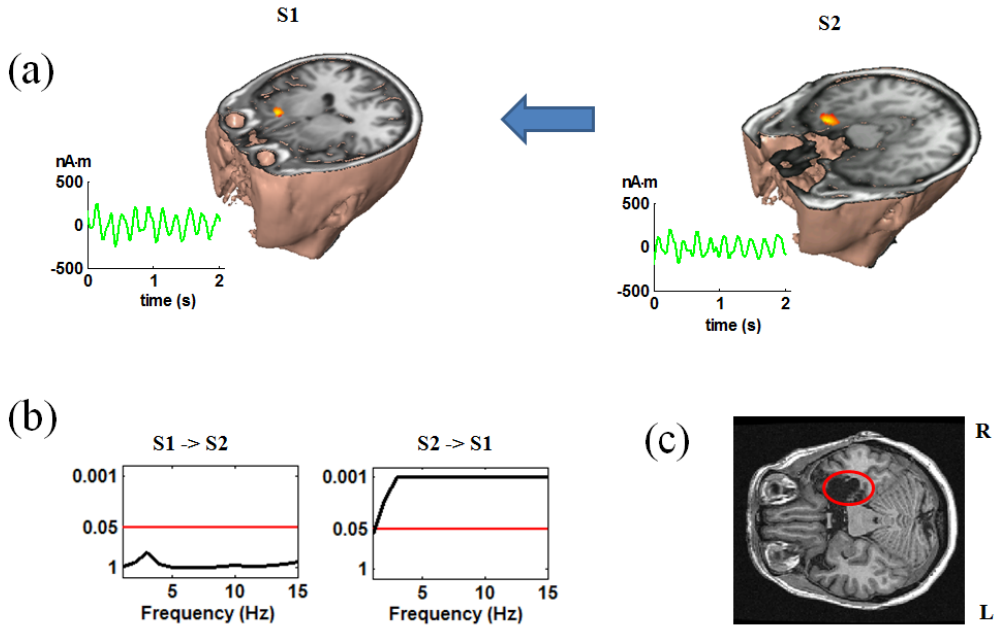

Fig. 3.4 Source imaging results of Patient 2. (a) Waveforms, locations, and directional causality of two sources (S1, S2). (b) Significance level of directional DTF values between S1 and S2. (c) Surgically resected area on post-operative MR image. Patient 2 had right temporal lobe epilepsy.

Patient 2 was a 50-year-old female with right temporal lobe seizures. One ictal period was captured from this patient during the long-term video monitoring. Rhythmic activities can be observed over the right hemisphere channels of the patient's scalp EEG during the seizure onset period. This patient underwent right temporal lobe lobectomy. The EEG source imaging results of Patient 2 are shown in Fig. 3.4. The two sources identified in this patient are located in right frontal lobe (S1) and right temporal lobe (S2).

The location and extent of these two sources are displayed in Fig. 3.4a along with the pre-operative structural MRI of the patient. The waveform of the source activity is also shown next to the two source locations in Fig. 3.4a. The connectivity analysis results in Fig. 3.4b show significant information flow from S2 to S1. Accordingly, the primary source identified in this patient was identified as S2, which is localized in the right temporal lobe. Fig. 3.4c shows the post-operative MR image with surgically resected area circled in the right temporal lobe.

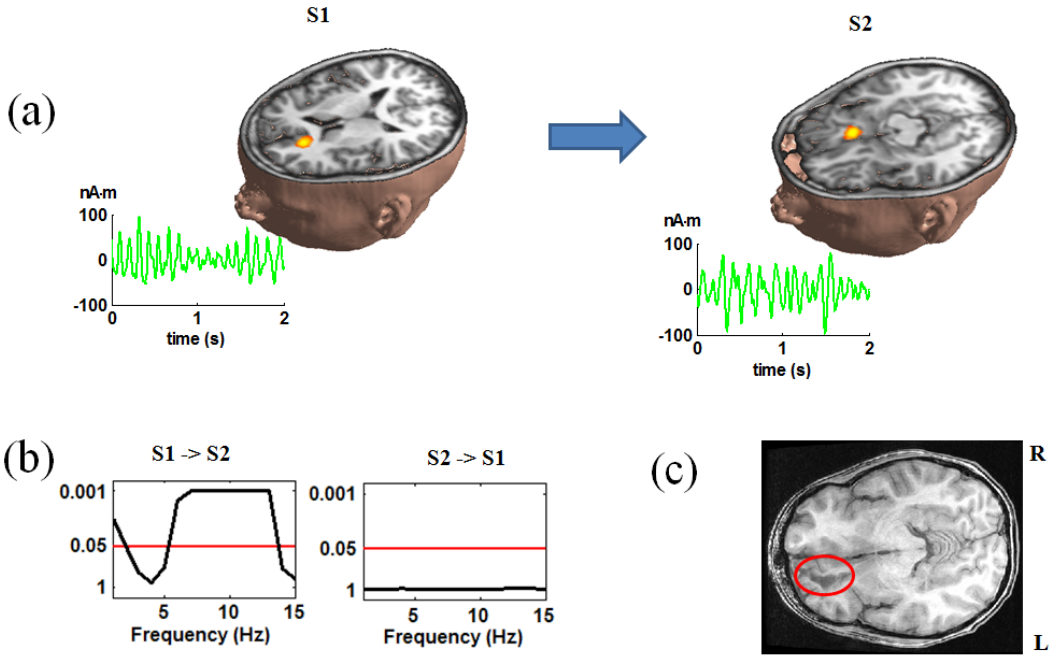

Fig. 3.5 Source imaging results of Patient 3. (a) Waveforms, locations, and directional causality of two sources (S1, S2). (b) Significance level of directional DTF values between S1 and S2. (c) Surgical resection on post-operative MR image. Patient 3 had left frontal lobe epilepsy.

Patient 3 was a 22-year-old female suffering from left frontal lobe seizures. Three seizures were captured from this patient during pre-operative long-term video EEG monitoring. This patient completed a left frontal cortectomy. Rhythmic activities can be

observed in the frontal EEG channels during ictal period of the patient. The EEG source imaging results of Patient 3 are shown in Fig. 3.5. FINE identified two sources (S1, S2) in the frontal lobe. S1 is in the left frontal lobe and S2 in the right frontal lobe close to the midline. Source locations and activities are shown together with the pre-operative MRI in Fig. 3.5a. Significant information flow from S1 to S2 is found over the 6-13 Hz frequency band in results of Fig. 3.5b. The results indicated that S1 is the primary source and is located in the left front lobe, which is in the same area as the surgical resection area (Fig. 3.5c).

Table 3.2 Summary of source image results in all 23 seizures of the ten patients. The estimated sources are compared with surgical resection of the patients.

	PT 1	PT 2	PT 3	PT 4	PT 5	PT 6	PT 7	PT 8	PT 9	PT 10
+	4	1	2	1	1	1	0	1	2	3
++	0	0	1	1	0	2	1	0	1	0
+++	0	0	0	0	0	1	0	0	0	0
Total	4	1	3	2	1	4	1	1	3	3

+: within 10 mm distance to the surgical resection boundary. ++: within 20 mm distance to the boundary. +++: within 25 mm distance to the boundary.

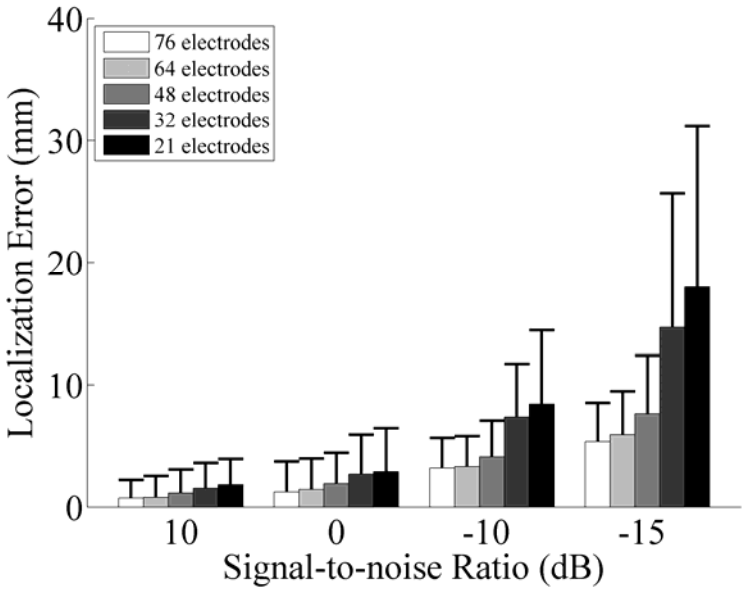

Fig. 3.6 Mean and standard deviation of localization errors in computer simulation. Localization errors of different electrode configurations (76, 64, 48, 32, and 21 electrodes) are coded in colors (from white to black). Simulation results in different noise levels are separated in groups.

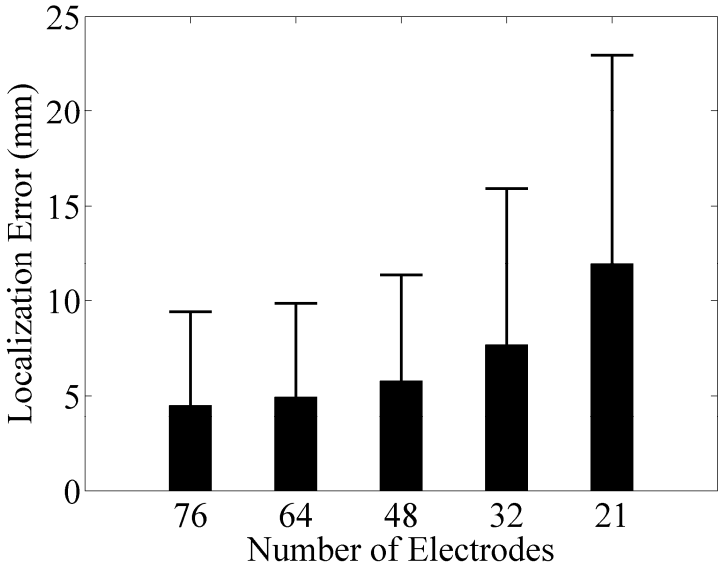

Fig. 3.7 Mean and standard deviation of localization errors in clinical data analysis.

The results in all the 23 seizures of the ten patients were shown in the Table 3.2. Source imaging results in the rest of the patients were also concordant with the surgically resected areas shown in post-operative MRI images. To quantitatively evaluate the source imaging results, group level analysis of localization error was performed on all the patients by calculating the distance between the estimated source and surgically resected boundary. To study the effect of electrode number in source imaging, we compared the results of different electrode configurations from both computer simulation and patient data.

Fig. 3.6 shows the localization error of the computer simulation using different electrode configurations and noise levels. Localization errors in the computer simulation were defined as the distance between estimated source and simulated source. Significant group difference (ANOVA, $p<0.01$) of localization error exists among all the different

electrode configurations (76, 64, 48, 32, and 21 electrodes). In low noise level condition (SNR=10 dB), a significant paired difference (t-test, $p<0.05$) of localization error is observed between any pairs of 64, 48, 32, and 21 electrodes. A significant paired difference can also be observed between 76 electrodes and other configurations (48, 32, and 21 electrodes). When SNR is 0 dB, a significant paired difference ($p<0.05$) is found between pairs of 76, 64, 48, and 32 electrodes. Significant paired difference can also be found between high density configurations (76, 64, and 48 electrodes) and 21 electrodes. In intermediate noise level condition (SNR=-10 dB), a significant paired difference ($p<0.01$) is observed between pairs of 64, 48, 32, and 21 electrodes. Significant paired difference can also be observed between 76 electrodes and other configurations (48, 32, and 21 electrodes). In high noise level condition (SNR=-15 dB), significant paired difference ($p<0.01$) exists between any two pairs of all the electrode configurations. These computer simulation results suggest that localization error increases as the number of electrodes is reduced. Under higher noise level, the localization errors are larger and more significantly distinguishable between different electrode configurations. This indicates the importance of using dense-array configurations in real conditions.

Fig. 3.7 shows the group level analysis of localization error in all the patient ictal data. Localization errors in clinical data represent the distance between the estimated source and surgically resected boundary. In patient results, larger localization error is also observed in fewer electrode configurations. Statistical t-test shows that the localization error is significantly smaller ($p<0.01$) in higher density configurations compared to configuration with 21 electrodes. The high density electrode configurations (76, 64, and

48 electrodes) show a significant paired difference ($p<0.05$) compared to configuration with 32 electrodes. An improving trend for localization can be observed by changing electrode configurations from 48 to 64 channels and from 64 to 76 channels. A significant paired difference ($p<0.1$) can also be observed between configurations with 76 and 48 electrodes. The ANOVA test shows a significant group difference ($p<0.05$) of localization error among all electrode configurations. Clinical data analysis presents the significant improvement of EEG source localization by increasing EEG signal channels from low density to high density electrode configurations. The most significantly improved source imaging result is observed in configurations with 76 electrodes. These results demonstrate the importance of applying high-density EEG in source imaging and suggest that it is necessary to use dense array EEG for high resolution source imaging.

3.4 Discussion

Despite the development and clinical application of various imaging techniques, accurately localizing epileptogenic zones in pre-surgical workup of medically intractable epilepsy remains to be vitally important. Intracranial recordings utilizing subdural grids and depth electrodes are currently the gold standards of identifying the position and extent of epileptogenic zones. Due to the limited spatial coverage and invasive nature of intracranial grids, many noninvasive functional neuroimaging techniques (PET, SPECT, fMRI) have been developed to enhance pre-surgical planning. Each of these functional neuroimaging techniques enables the capture of additional useful information for pre-surgical workup and, ultimately, enhanced outcomes of epilepsy patients. However, these

extant techniques have poor temporal resolution and may not indicate the precise epileptogenic zone, but rather regions of seizure propagation. On the other hand, EEG represents a direct measurement of brain electrophysiological activities and has a high temporal resolution (at millisecond scale), which makes it possible to study the initiation and propagation of epileptiform discharges and seizure activities. Long-term video EEG monitoring is now available as a routine procedure in most clinical centers, and could be a more useful pre-surgical evaluation tool when coupled with source analysis techniques.

Many attempts have been made to study the application of noninvasive EEG source imaging techniques for localizing epileptic sources. Cortical potential imaging techniques was applied in epilepsy patients and found the consistency between epileptic cortical areas and surgical resections (Zhang et al., 2003; Lai et al., 2011). Good performance of equivalent current dipole modeling was demonstrated in source analysis of temporal and frontal lobe epilepsy (Gavaret et al., 2004, 2006). Parameterization of ictal data in time domain or frequency domain was also applied to study ictal source analysis (Worrell et al., 2000; Morlet and Gotman, 2001; Lantz et al., 2001; Boon et al., 2002). The approach applied in this study combines spatio-temporal source localization and source connectivity analysis for seizures. This integrative approach is capable of characterizing causal information flow between different sources and discriminating the primary ictal source from propagated sources.

An important issue in EEG source imaging is modeling source configurations and choosing inverse algorithms. Dipolar source model and distributed source model are the most commonly used source models in EEG source imaging (He et al, 2002; Michel et

al., 2004). The assumption for dipolar source model is that a few discrete sources are adequate to explain the scalp potential. Studies have shown that equivalent current dipolar source model can be successfully applied in localizing focal epileptiform activities (Assaf and Ebersole, 1997; Gavarat et al., 2004). However, *a priori* knowledge of the source number is usually hard to determine and dipolar models cannot adequately represent the extent of the sources, despite efforts on estimation of the number of dipoles (Bai and He, 2005, 2006). In distributed source models, current sources are located in the whole source space such as 3D brain volume or 2D cortical surface. Various inverse methods were successfully employed to image the electrical sources of epilepsy patients (Assaf and Ebersole, 1997; Gavarat et al., 2004; Michel et al., 2004; Holmes, 2008). To utilize EEG source analysis as a pre-surgical evaluation tool in clinical procedure, more studies are needed to investigate the feasibility of source imaging approaches in localizing epileptogenic foci of epilepsy patients.

Due to the availability and feasibility of dense array EEG recording systems, high-density EEG source imaging has been attracting more and more attention from epilepsy researchers and clinicians. Studies have shown that more recording electrodes allow for accurate epileptic source localization results (Lantz, et al., 2003). A great precision in localizing interictal epileptic activity was reported by applying high-density EEG source imaging in epilepsy patients (Michel et al., 2004). Dense array EEG has also proved useful in noninvasive ictal localization for both generalized and localization-related seizures (Holmes, 2008). In contrast to routine scalp EEG recordings in current clinical settings, which only use 19-21 recording electrodes, in this study we utilized high-density

EEG with 76 channels to localize ictal onset zones with high resolution. We also compared the source imaging results in different electrode configurations by downsampling 76 channels into 64, 48, 32, and 21 channels. Our results demonstrated the significant improvement of EEG source localization by increasing the electrode numbers. That is, the most significantly improved result was observed in configurations with 76 electrodes. The potential application of high-density EEG may provide more information than the traditional scalp EEG recordings and help lateralizing or localizing epileptogenic zones.

Epilepsy patients with partial seizures usually limit their seizure activities in a few focal regions of the brain. In this study, seizure source imaging was successfully applied to ten partial epilepsy patients in localizing their epileptogenic zones. In extratemporal patients or other epilepsy patients, seizure activities may start from more brain regions and involve with larger brain networks. Studies in different epilepsy types in the future may be interesting and meaningful to extend the seizure imaging in more complex epilepsy types. While the nature of the present study involves a substantial amount of work including high density EEG recordings, seizure source imaging and comparison with surgical resection outcomes, the study is limited in its patient population. Future studies in larger patient groups may still be needed to assess the high-density EEG recording and seizure imaging in localizing epileptogenic zones.

In summary, we applied the FINE approach to noninvasively localize the seizure activities of medical intractable partial epilepsy patients. High-density EEG recordings together with patient specific BEM head models were utilized to improve the spatial

resolution of the source imaging. Furthermore, Granger causality analysis using DTF was used to further define the primary seizure sources. Our source imaging results in the ten epilepsy patients showed high co-localization with their surgical resections. We further compared the performance of source imaging from different numbers of electrodes. Computer simulation and clinical data analysis showed the improvement of EEG source imaging as a result of increasing the number of electrodes. Overall, the present study demonstrates the feasibility of high-density EEG recordings and high resolution ictal source analysis in localizing ictal onset zones and indicates its potential usage in pre-surgical planning of epilepsy patients.

Chapter 4 Dynamic Imaging of Continuous Seizure Activities in Pediatric Patients

4.1 Introduction

Epilepsy is one of the most important chronic neurological diseases that affect children. Approximately 0.5% to 1% of all children under 16 years experience seizure events (Shinnar and Pellock, 2002). Children that suffer from epilepsy may face intellectual developmental issues and encounter other brain developmental problems. Seizure control and treatment are of vital importance to pediatric patients in order to improve their quality of life as well as ensure normal brain development. In contrast to adult patients, pediatric patients are more likely to experience seizures that originate from extratemporal lobe regions, which tend to have a less favorable surgical outcome compared to temporal lobe epilepsy (Gilliam et al., 1997; Sperli et al., 2006). It is thus important to accurately localize the epileptogenic zone of pediatric epilepsy patients in order to achieve improved surgery success.

Pre-surgical planning techniques from multiple aspects are necessary in order to plan a successful surgical resection. Among various techniques, intracranial recordings including electrocorticography (ECoG) and depth electrodes are still the gold standards to identify the seizure onset zones (Engel, 1987; Lai et al., 2007; Wilke et al., 2009, 2010, 2011). However, as iEEG has been restricted by its invasive nature and limited spatial coverage, noninvasive structural and functional imaging techniques, such as magnetic resonance imaging (MRI), positron emission tomography (PET), and single photon emission computed tomography (SPECT), have been actively developed and utilized to

delineate the epileptogenic zones. Due to the limited temporal resolution and uncertain correlation between the imaging response and neuronal activities, these techniques alone may not provide sufficient information to identify the seizure onset zone. Additional information from other imaging modalities is thus necessary to fully understand the epileptic brains and identify the epileptogenic zones.

Scalp EEG has been widely used in clinical settings to characterize seizure activities in epilepsy patients. Patients typically undergo long-term video monitoring to capture their seizures and to help lateralize or localize seizure onset regions. Recent advancement in the EEG source imaging technique has made it possible to study the activities in the brain source space in addition to the traditional scalp EEG trace inspection. Many studies have shown the capability of EEG source imaging in localizing the brain sources in interictal epileptiform discharges (He et al., 1987; Ebersole, 2000; Lantz et al., 2003; Zhang et al., 2003; Michel et al., 2004; Gavaret et al., 2004; Sperli et al., 2006; Plummer et al., 2008; Brodbeck et al., 2010; Wang et al., 2010; Lai et al., 2011). The imaging of seizure activities still remains a challenge due to the various types of ictal patterns and contamination of moving artifacts in EEG (Assaf and Ebersole, 1997; Worrell et al., 2000; Lantz et al., 2001; Ding et al., 2007; Koessler et al., 2010; Yang et al., 2011). Among the seizure imaging studies, temporal lobe epilepsy is the most investigated epilepsy type. Few studies have evaluated results with surgical resection as well as intracranial recordings in pediatric patients. In this study, we investigate the feasibility of using a dynamic seizure imaging technique to identify seizure generators in pediatric epilepsy patients (Lu et al., 2012b). To evaluate the source imaging results, we

compare the estimated source with both surgical resections and intracranial recordings of the patients.

4.2 Methods

4.2.1 Patients and data analysis

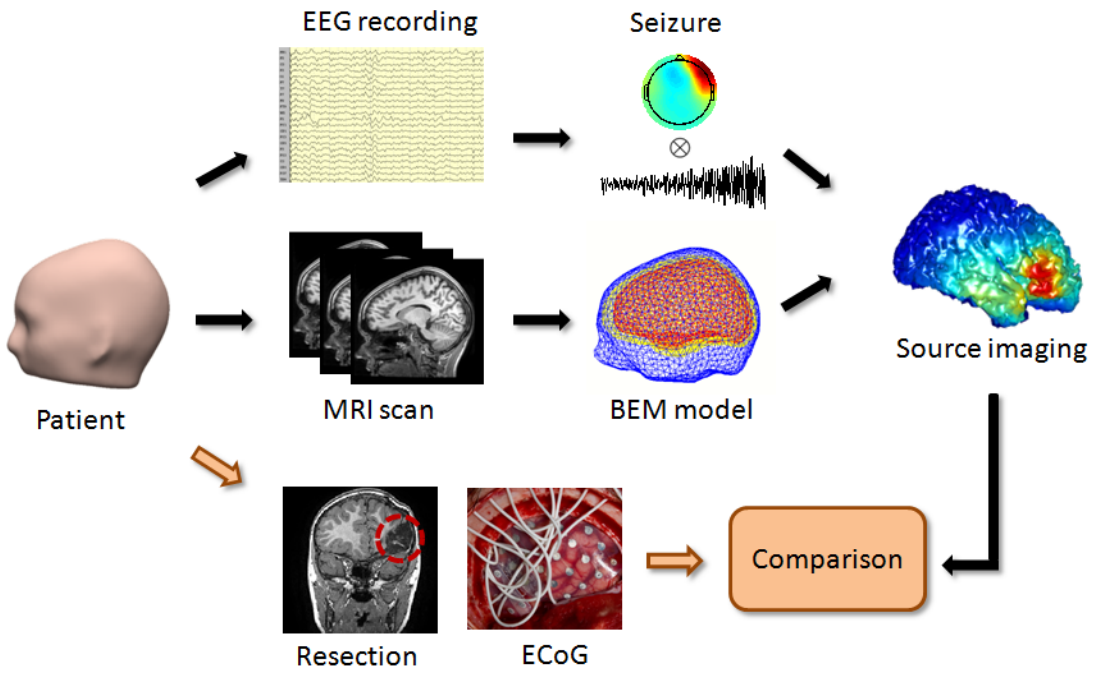

Fig. 4.1 Schematic diagram of seizure source imaging and the study design. Seizure activities from scalp EEG recordings are analyzed to image seizure sources. Patient-specific BEM models are created from pre-operative MRI images of the patients. Surgical resections and intracranial recordings are used to evaluate the seizure source imaging results.

Table 4.1 Clinical information for all patients.

Patient	Age at onset	Age	MRI	SPECT	Scalp EEG	Ictal symptoms	Seizure duration	Surgery	Pathology	Outcome	Follow-up (month)
1	10 months	2	Normal	Inferolateral right frontal lobe; left inframedial occipital lobe	Paroxysmal fast activity maximally at Fp2, F8, and F4	Brief head flexion; turning to the right	20 s	Right lateral and inferior frontal cortical resection	Focal cortical dysplasia	ILAE-1	15
2	1 month	16	Parieto-occipital encephalomalacia	Anterior commissure, right intraparietal sulcus, and lateral left occipital lobe	Rhythmic theta activity near left posterotemporal and occipital head region	Confusion with cessation of activity; automatisms of the upper extremities; vocalization	80 s	Left occipital resection	Severe neuronal loss; gliosis; focal dystrophic calcification	ILAE-1	16
3	-	18	left frontal cortical dysplasia or subcortical gliosis	-	Rhythmic alpha activity over left central region	Felt weird; points to the tongue; involuntary tongue movements	2 min	Cortical resection of seizure focus	Focal cortical neuronal loss; gliosis	ILAE-3	7
4	7	9	Mild Chiari I malformation	Mild increase in anterior right cingulate cortex	Left frontal and left anterior temporal head region with rhythmic alpha frequency spikes	Arouse from sleep; extend right arm; abduct left arm	30 s	Resection of left frontal, left frontal interhemispheric cortex	Mild gliosis; Malformation of cortical development	ILAE-1	8
5	6	17	Normal	No clear focus	Rhythmic discharge at right frontal and midline frontal	Left facial tonic contraction; forced head turn to left	1 min	Right superior lateral and superior medial frontal cortical resection	Severe gliosis predominantly subcortical and subpial	ILAE-5	12
6	13	16	Normal	Mesial right temporal, right frontal cortex, and right basal ganglia	Rhythmic theta activity over the right parietal, midline central, and right temporal region	Behavioral arrest; subtle non-forced head turn to right; unresponsive to questioning	40 s	Right frontocortical resection; Right temporal lobectomy	Mild subpial and subcortical gliosis	ILAE-1	9
7	5	10	Right frontal hemorrhage related to cavernoma	Bilateral left more than right frontal, and right temporal lobe	Broad sharp right frontal discharge	Elevated left arm; left upper extremity clonic movement; forced head turn to the left	50 s	Right anterior frontal lobectomy	Gliosis, subcortical and subpial	ILAE-4	12
8	7	12	Left hippocampal atrophy	-	Delta frequency activity over the left temporal region maximal at T7 and T9	Brief speech impairment and gesturing; "scared feeling" in stomach	1 min	Left anterior temporal lobectomy; Amygdalohippocampectomy	Mild subpial and subcortical gliosis; Mesial temporal sclerosis	ILAE-1	8
9	4	5	Normal	-	Polyspike discharge in left parietal region at P3	Head and body turn to the right	30 s	Left parietal cortical resection	Gliosis, subcortical and subpial	ILAE-4	15

The study design is illustrated in Fig. 4.1. Nine pediatric patients with drug-resistant partial epilepsy were included in this study. The pediatric patients were selected according to the following criteria: (1) seizures were captured during the long-term EEG recording, (2) pre-surgical MRI images were scanned, (3) the patient underwent resective surgery and the age of patient was below nineteen when the surgery was performed, (4) the patient had either a post-operative MRI scan or intracranial recordings. The patients were studied under the approved protocol by the Institutional Review Boards of the University of Minnesota and the Mayo Clinic. The clinical information for these patients is included in Table 4.1.

The pre-surgical scalp EEG of these patients was recorded in a long-term video monitoring system. The EEG data were filtered with a band-pass filter of 1-70Hz and sampled at 200 Hz. The scalp EEG was recorded with 32 channels and the electrodes were positioned according to the modified international 10-20 system. The EEG data were carefully reviewed and seizures marked by experienced epileptologists. A total of 32 seizures from the patients were analyzed using the dynamic seizure imaging approach. High resolution structural magnetic resonance imaging was also performed in all of these patients before their surgery. These MRI images (voxel size: 0.9375* 0.9375* 1.0 mm^3) were obtained from a 1.5 Tesla or 3 Tesla GE Signa scanner (General Electric Medical Systems, Milwaukee, WI). Patient-specific realistic geometry boundary element method (BEM) head models were constructed from the MRI images using Curry software (Compumedics, Charlotte, NC).

4.2.2 Dynamic seizure imaging

The dynamic seizure imaging (DSI) approach separates the scalp EEG into independent components (ICs) in sensor space and recombines seizure components in the source space to form a spatiotemporal reconstruction of seizure activity (Yang et al., 2011). The scalp EEG is a mixture of activities from various sources, which include functional cortical activations, background brain activities, artifacts and noises. In the analysis, seizure EEG can be separated into temporally independent and spatially fixed components using the independent component analysis (ICA) in the following format (Nam et al., 2002; Delorme and Makeig, 2004; Jung et al., 2009; Yang et al., 2011)

$$\Phi = \mathrm{WMT} = \sum_{i=1}^{N_C} w_i M_i T_i \tag{4.1}$$

where Φ is the recorded scalp EEG, N_C is the number of independent components, w_i is the *i*th weighting element, M_i and T_i represent the spatial map and temporal activation of *i*th component, respectively.

Components that correspond to artifacts, such as eye blinks and moving artifacts, were removed from the decomposed ICs (Jung et al., 2000). Components characterized by temporal-spectral patterns of ictal activities were selected for the source analysis. Correlations of spectrogram between IC components and scalp ictal EEG were computed. The spectrogram was calculated using a short-time Fourier transform with the time window of 200 samples and 50% overlapping. The empirical correlation distribution was then created for each IC by computing the spectrogram correlation of surrogated IC time series and EEG data (Yang et al., 2011). The ICs with significant correlation ($p < 0.1$) in the surrogated statistical test were selected. The IC components with more than 20%

residual variances of dipole fitting were excluded for the seizure source imaging (Delorme and Makeig, 2004; Jung et al., 2009). After selecting the seizure components in Eq. (1), the ictal EEG Φ can be written as $\sum_{i=1}^{N_S} w_i M_i T_i$ (where N_S is the number of seizure components).

By solving the inverse problem, the estimated source activities $\hat{S}$ can thus be expressed as

$$\hat{S} = A^{-1}\Phi = A^{-1}\left(\sum_{i=1}^{N_S} w_i M_i T_i\right) = \sum_{i=1}^{N_S} w_i \left(A^{-1} M_i\right) T_i \approx \sum_{i=1}^{N_S} w_i \hat{S}_i T_i \qquad (4.2)$$

where A^{-1} is the inverse of transfer matrix A, $\hat{S}_i = A^{-1} M_i$ is the estimated source for *i*th seizure component. The spatiotemporal source distribution $\hat{S}$ could then be obtained by combining the IC sources $\hat{S}_i$ and time courses T_i in the source domain. To estimate the $\hat{S}_i$, cortical current density model with unconstrained sources (Dale and Sereno, 1993) and minimum norm estimation (Hämäläinen and Ilmoniemi, 1984) were used to reconstruct the source distribution. The cortex was segmented from high-resolution structural MRI of the patients, and the transfer matrix was computed from patient-specific realistic geometry BEM head model (Hämäläinen and Sarvas, 1989). The BEM model consisted of three layers (scalp, skull, brain) and the conductivities were set as 0.33 S/m, 0.0165 S/m, and 0.33 S/m, respectively (Lai et al., 2005; Zhang et al., 2006).

2.3 Evaluation of imaging results

The seizure imaging results were obtained from the nine patients and the results were compared with the surgical resection of the patients. The estimated seizure sources

were distributed over the cortical surface, and the cortical source location with the maximal source strength was considered as the location of the estimated seizure activities. All the patients had both resective surgery and post-operative MRIs following the surgery. The surgically resected areas were segmented from the post-operative MRI images and used to evaluate the DSI results. The results were considered to be concordant to surgical resection if the estimated source maximum was located within the resection regions.

In the seven patients with intracranial recordings, we quantitatively evaluated the seizure imaging results at seizure onset by comparing the location of estimated sources with the SOZs of intracranial recordings. The SOZs were identified from ECoG electrodes by experienced epileptologists. The accurate locations of intracranial electrodes were segmented from CT images and co-registered with structural MRI images. The distance between the estimated source maximum and nearest SOZ electrode was calculated. The unit of the distance was defined as the inter-electrode-distance, which was the distance between two adjacent ECoG electrodes. The estimated seizure activities following seizure onset were also displayed and qualitatively compared to iEEG recordings.

4.3 Results

Nine pediatric patients with medically intractable epilepsy were analyzed in this study. Among the nine patients, eight of them experienced extratemporal lobe seizures and one of them had temporal lobe seizures. Seizure imaging results in all patients were evaluated by comparing them with surgical resection zones of the patients. In seven

patients who had intracranial ECoG recordings, the estimated sources were also compared with the SOZ of intracranial recordings.

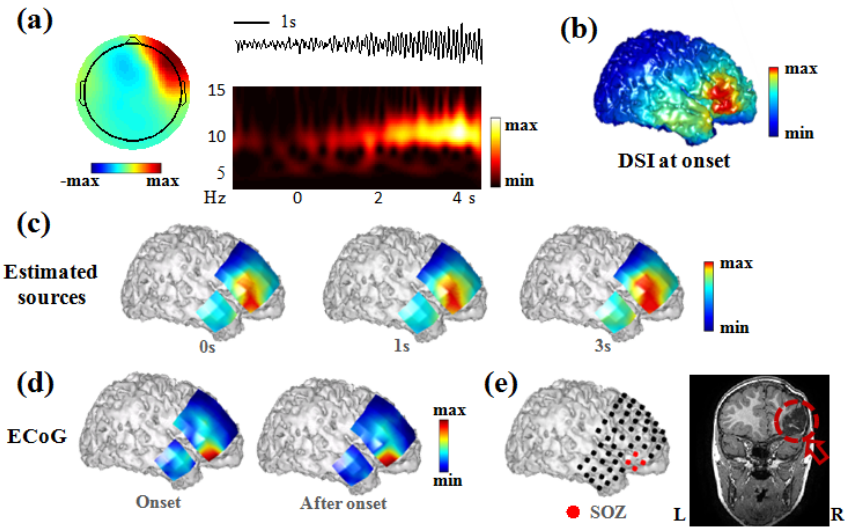

Fig. 4.2 Seizure source imaging results in Patient 1. (a) Example of scalp topography, activity, and time-frequency representation of one seizure component. (b) Estimated source at seizure onset. (c) Estimated seizure sources following seizure onset. The estimated sources were displayed by projecting them onto the cortical grid surface. (d) Power distribution of recorded ECoG activities following seizure onset. (e) Seizure onset zone (red color) marked on ECoG grid and surgical resection circled on post-operative MRI image of the patient.

Patient 1 was a 2-year-old patient who had extratemporal lobe seizures. The seizures were characterized as paroxysmal fast activities in the frontotemporal head region. Fig. 4.2 shows the seizure imaging results of this patient in comparison with the surgical resection and the intracranial recording. Multiple seizure components were extracted and the seizure component showing the earliest ictal activation is shown in Fig. 4.2a. The scalp map suggests right fronto-temporal focus of the activity. Both the time course and time-frequency representation show source activity at the alpha frequency band following the onset of the seizure. The cortical distribution of the estimated seizure

activity (Fig. 4.2b) indicates seizure onset in the right lateral frontal region. Intracranial recordings were performed on this patient, which covered the right frontal lobe and right temporal lobe of the patient. Part of the estimated cortical source distribution that overlaps with the intracranial grids is plotted and projected onto the grid surface (Fig. 4.2c). Both estimated seizure sources, and the power distribution of recorded ECoG activities (Fig. 4.2d) show that the seizure was consistently active in the right lateral frontal lobe. The seizure onset zone marked on Fig. 4.2e shows that the seizure started from the right frontal grid of this patient. The red circle on the post-operative MRI image (Fig. 4.2e) shows that part of the right frontal lobe was removed during the surgery. These results suggest that the estimated seizure source in the right frontal lobe is in concordance with the surgically resected region and the SOZ delineated from intracranial electrodes.

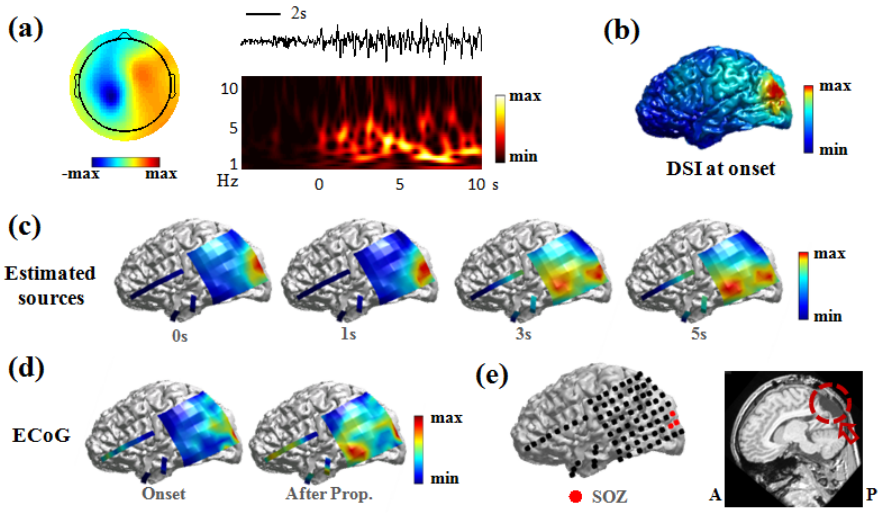

Fig. 4.3 Seizure source imaging results in Patient 2. (a) Example of scalp topography, activity, and time-frequency representation of one seizure component. (b) Estimated source at seizure onset. (c) Estimated seizure sources following seizure onset. The estimated sources were displayed by projecting them onto the cortical grid surface. (d) Power distribution of recorded ECoG activities at seizure onset and after propagation. (e) Seizure onset zone (red color) marked on ECoG grid and surgical resection circled on post-operative MRI image of the patient.

Patient 2 was another extratemporal lobe patient whose seizure activities involved multiple brain regions. The scalp EEG of the analyzed seizure showed occipital and temporal lobe activities. Multiple seizure components were extracted and the seizure component showing the earliest ictal activation is shown in Fig. 4.3a. The spatial map indicates parieto-occipital lobe focus of seizure activities. The time course and time-frequency representation show seizure activities in theta band following the seizure onset. The estimated seizure onset source over the cortex (Fig. 4.3b) shows that the seizure sources were activated in the occipital lobe of the patient. The seizure onset zone marked in Fig. 4.3e shows that the seizure started from the occipital region of this patient. The

post-operative MRI image in Fig. 4.3e shows that part of the occipital region of this patient was resected during the surgery. The estimated sources in Fig. 4.3c show that the seizure sources were firstly activated in occipital lobe and then sources in the posterior temporal lobe were also activated, which was confirmed by the power distribution of recorded seizure activities from intracranial electrodes (Fig. 4.3d). The seizure development involving multiple regions was successfully tracked by the seizure imaging approach. The estimated seizure onset source is located in the left occipital region and it is concordant with the surgical resection and SOZ of the intracranial recording.

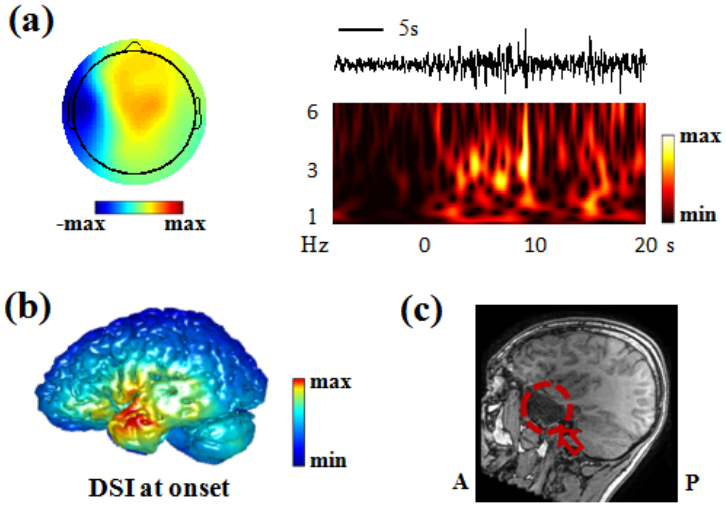

Fig. 4.4 Seizure source imaging results in Patient 8. (a) Example of scalp topography, activity, and time-frequency representation of one seizure component. (b) Estimated source at seizure onset. (c) Post-operative MRI image of the patient. The surgical resection is marked by red circle.

Patient 8 was an epilepsy patient with temporal lobe seizures. The scalp EEG of the patient showed delta frequency activities over the left temporal region. Multiple seizure components were extracted and the seizure component showing the earliest ictal

activation is shown in Fig. 4.4a. The spatial map indicates left temporal seizure activities. The time course and time-frequency representation show seizure activity in the delta frequency band following the seizure onset. The estimated seizure sources in Fig. 4.4b show that the seizure source is active in the left temporal lobe of this patient. The post-operative MRI image of this patient (Fig. 4.4c) shows that part of the left temporal lobe was resected during the surgery. The estimated seizure source in the left temporal lobe is concordant with the surgical resection zone that is shown in the post-operative MRI image. Since the intracranial recording was not available in this patient, a comparison between the source imaging results and the SOZ was not performed.

Table 4.2 Source imaging results in all pediatric patients.

Pt	Surgery	Location of source maximum	Concordance to resection	Concordance to SOZ †
1	Right frontal lobe	Right posterior frontal	+	< 1
2	Left occipital lobe	Left occipital	+	< 1
3	Left frontal lobe	Left posterior frontal	++	~ 2
4	Left frontal lobe	Left superior frontal	+	~ 1
5	Right frontal lobe	Right superior frontal	+	~ 1
6	Right frontal/right temporal lobe	Right superior frontal	+	~ 1
7	Right frontal lobe	Right anterior frontal	+	~ 3
8	Left temporal lobe	Left temporal	+	N/A
9	Left parietal lobe	Left parietal	++	N/A

+: Source maximum is located inside surgical resection; ++: Source maximum is close to surgical resection; †: Concordance to SOZ is defined as the distance from source maximum to SOZ in the unit of inter-electrode-distance of ECoG electrodes. Comparison to SOZ are N/A in two patients because the intracranial recordings were not available in these two patients.

The seizure imaging results in all nine epilepsy patients are summarized in Table 4.2. The source imaging result is considered to be concordant to surgical resection if the estimated source maximum is located within the resection zones. In seven of the nine

patients, the estimated source maxima were located inside the surgical resection zones. The estimated source maxima of the other two remaining patients were within 2 cm distance to the resection boundary. Intracranial recordings are available in seven of the nine patients. In five patients, the estimated source was either smaller than one or only one inter-electrode-distance away from the SOZ. It is worthwhile to note that a distance smaller than 1 inter-electrode does not necessarily indicate a localization error, because activities between two electrodes cannot be directly measured by the iEEG. The average distance to SOZ of the seven patients is 1.4 inter-electrode-distances. These results demonstrate that the seizure imaging results are co-localized with the surgical resection and intracranial recordings of the studied patients.

4.4 Discussion

Long-term EEG monitoring can non-invasively capture seizure activities with more spatial coverage. The advancement of source imaging approaches has made it possible to study the underlying brain source activities in addition to the traditional EEG trace interpretation. Several source analysis methods have been applied to study ictal activities of epilepsy patients (Assaf and Ebersole, 1997; Lantz et al., 1999; Worrell et al., 2000; Merlet and Gotman, 2001; Koessler et al., 2010; Holmes et al., 2010). However, the localization of seizure activities remains challenging because ictal EEG signals are usually contaminated by artifacts and noise. The ictal discharge can change in time, space and frequency, which increases the difficulty for the source imaging. To separate the spatial, temporal and spectral patterns from seizure activity, blind source separation techniques (Nam et al., 2002; Patel et al., 2008; Jung et al., 2009) have been

used to decompose seizure activities into independent components. Along this line, a dynamic seizure imaging approach (Yang et al., 2011) has recently been developed to image the continuous change of ictal activities. Instead of solving the inverse problem on discrete EEG time instants, the dynamic seizure imaging approach extracts seizure components with temporal-spectral features and recombines the components in the source domain to form a spatiotemporal imaging. In this study, the dynamic seizure imaging approach was applied in nine pediatric patients and DSI was able to extract the activities of seizure sources. The estimated seizure sources were consistent with surgical resections and intracranial recordings of the patients.

EEG source imaging techniques can noninvasively study brain activities by modeling the brain sources and volume conductor (He et al., 1987; Michel et al., 2004; Plummer et al., 2008; He et al., 2011). In the study, a patient-specific BEM head model was obtained from individual MRI and used for EEG source analysis to improve the spatial resolution. Studies have shown that more precise source localization results can be obtained in realistic-geometric head models compared to simple spherical head models (Herrendorf et al., 2000; Wang et al., 2010). The performance of EEG source imaging could further be improved by incorporating more *a prior* information such as anisotropic conductivities (Michel et al., 2004) and fMRI constrains (He & Liu, 2008; Liu and He, 2008; Yang et al., 2010) of the patients. Future studies in more sophisticated finite element method head models and fMRI-constrained EEG may be necessary to further improve the application of EEG source imaging in epilepsy patients.

While adult epilepsy patients are more likely to experience temporal lobe seizures, pediatric epilepsy patients suffer more from extratemporal epilepsy (Gilliam et al., 1997; Sperli et al., 2006). The overlapping of the epileptogenic zone and the functional brain region make it more difficult to achieve favorable surgical outcome in extratemporal cases without jeopardizing eloquent function of patients. As a result, it is more important yet challenging in pediatric patients to correctly differentiate the epileptogenic zone from normal brain tissues. Among the eight studied extratemporal epilepsy patients, the estimated seizure onset results of six patients were located within the resected region. In the remaining two patients with parietal and frontal seizures, the estimated source maxima were not located within the resected region but very close to the boundary of the resection. This could be the localization error of EEG source imaging and could also be explained by the limited resection size in these two patients. These two patients were not seizure free, which means that the epileptogenic zone was not completely resected in the surgery. Although it is important to remove the entire epileptogenic zone to obtain a seizure free outcome, resective surgery has to be conservative in extratemporal patients to preserve functional brain areas. Future studies of DSI in distinguishing functional brain regions could further help in separating eloquent cortex from pathological tissues and thus provide more information for surgical planning.

Another challenging problem in pre-surgical planning of epilepsy patients is to identify the epileptogenic zones in MRI-negative patients. With the advancement of MRI imaging techniques, more mild changes in brain structure could now be visible in MRI scans. However, it is not rare to have epilepsy patients with normal images in various

MRI scan sequences (Rosenow and Lüders, 2001; Brodbeck et al., 2010). Furthermore, the structural lesions visible in MRI may not be epileptic and the true epileptic brain tissue may exist in regions that are distinct from the MRI lesions. Noninvasive approaches localizing epileptic regions are thus extremely helpful in these MRI-negative patients. Among the nine patients included in this study, five of them have visible lesions and the remaining four patients have normal MRI images. The seizure imaging in three of these four MRI-negative patients shows concordant results with the surgical resections. While more studies are needed to further investigate the additional value of noninvasive EEG in MRI-negative patients, the results in our study suggest that the seizure imaging approach could potentially be helpful in localizing epileptic regions of pediatric patients with normal MRI.

In conclusion, we applied a spatiotemporal seizure imaging approach to localize the seizure activities of nine drug-resistant pediatric epilepsy patients. This approach studied the time-frequency seizure features and imaged the onset as well as the continuous activations of seizures. The dynamic study of seizures is important to epilepsy patients in order to better understand the seizure characteristics and mechanism. The estimated seizure sources in the present study were compared with the surgical resections and intracranial recordings of the patients. Concordant results were obtained by comparing the source locations with the resection regions and SOZ of intracranial electrodes. This study demonstrates that the seizure imaging technique can help to noninvasively localize seizure sources in pediatric patients. It also has the potential to

help guiding the implantation of intracranial electrodes and to provide additional information for pre-surgical planning of epilepsy surgery patients.

Chapter 5 Noninvasive Imaging of the High Frequency Brain Activity

5.1 Introduction

Epilepsy is a chronic neurological disorder affecting over 50 million people in the world. Patients with epilepsy are usually treated with antiepileptic drugs (AEDs) to control their seizures. However, about 30% of the patients do not respond to the medications and their seizures continue despite trying multiple AEDs (Cascino, 1994). Neurostimulation treatments may be performed in some medically resistant epilepsy patients to suppress seizures. However in the close-loop responsive cortical stimulation (Morrel, 2011), localizing the epileptogenic zone is important for guiding the implantation of brain stimulation leads. Surgical intervention is a viable option for the medically resistant focal epilepsy when seizures are impacting their quality of life and no AEDs or medical devices are controlling the seizures (Engel, 1987). Accurate localization of the epileptogenic zone thus plays a critically important role in guiding the resective surgery and in directing brain stimulation.

Despite considerable efforts made so far, it remains challenging to accurately identify the epileptogenic zone for favorable surgical outcome. Intracranial EEG (iEEG) recordings utilizing subdural grids and depth electrodes are still the gold standard of determining the seizure onset zone (SOZ) of epilepsy patients (Rosenow and Lüders 2001). However, intracranial recording is an invasive procedure and it involves risks such as cerebral hemorrhage and infection. Current clinical practice requires a prolonged recording for up to ten days in order to identify SOZ, which further increases the risks

and complications of this procedure. Furthermore, the intracranial recording has limited spatial coverage since only a limited portion of the cortical surface or brain regions can be covered by the intracranial electrodes (Lai et al., 2011; Wilke et al., 2010; Wilke et al., 2011). Structural magnetic resonance imaging (MRI) has also been widely used to image the abnormal structural lesions in epilepsy patients. However, the MRI lesion is not the ideal indicator of epileptogenic zone. Some patients may have multiple non-epileptic lesions while structural lesions may not be revealed with MRI in many other patients. Additional information from other modalities is thus much needed to further understand the epilepsy and to better delineate the epileptogenic zone.

High frequency (HF) brain oscillations are the recorded electrical activity ranging from 30 Hz to 500 Hz, and include gamma, ripple and fast ripple activity (Engel Jr. and da Silva 2012). Since the discovery of HF activity in epilepsy patients, many studies have suggested that HF activity may represent an effective biomarker of epileptogenicity (Bragin et al., 1999; Jacobs et al., 2012; Jirsch et al., 2006; Worrell et al., 2008; Worrell et al., 2012). Studies have shown that HF activity was strongly correlated to the SOZ, with significantly higher HF occurrence rates and durations inside the SOZ than the non-SOZ area (Crépon et al., 2010; Jacobs et al., 2008). The HF activity is also highly correlated with the follow-up outcome of epilepsy surgery (Akiyama et al., 2011; Ochi et al., 2007). Studies have shown that the complete removal of brain areas with HF activity was more likely to achieve a favorable surgical outcome in the epilepsy surgery (Jacobs et al., 2010; Wu et al., 2010).

EEG/MEG are the noninvasive recording of electrophysiological brain activity and

they have been widely used in research labs and clinical centers to help study functioning brain activity and pathological brain abnormalities (Astolfi et al., 2005; Astolfi et al., 2008; Bai and He 2006; Baillet et al., 2001; Billings et al., 2013; Ding et al., 2007a; Ebersole and Hawes-Ebersole 2007; Guggisberg et al., 2008; He et al., 1987; He et al., 2011a; He et al., 2011b; He and Ding 2013; He et al., 2013; Lai et al., 2011; Lantz et al., 2003; Lu et al., 2012a; Lu et al., 2012b; Michel et al., 2004; Sekihara et al., 2001; Van Veen et al., 1997; Wang and He 1998; Wilke et al., 2008; Yang et al., 2011; Yang et al., 2012; Zhang et al., 2003). EEG has been routinely recorded in epilepsy centers to identify interictal activity or seizure activity to diagnose and classify epilepsy. Recent studies have also shown that HF activity can be recorded from scalp EEG in both children and adult epilepsy patients (Andrade-Valenca et al., 2011; Kobayashi et al., 2011). HF activity on scalp EEGs including gamma and ripples were frequently associated with spikes and their occurrences were much higher within than outside of the seizure onset zone (Andrade-Valenca et al., 2011). Since the HF activity can be recorded in scalp EEGs, studies estimating the underlying sources of HF activity are desirable to further investigate the feasibility of noninvasively localizing epileptogenic zone.

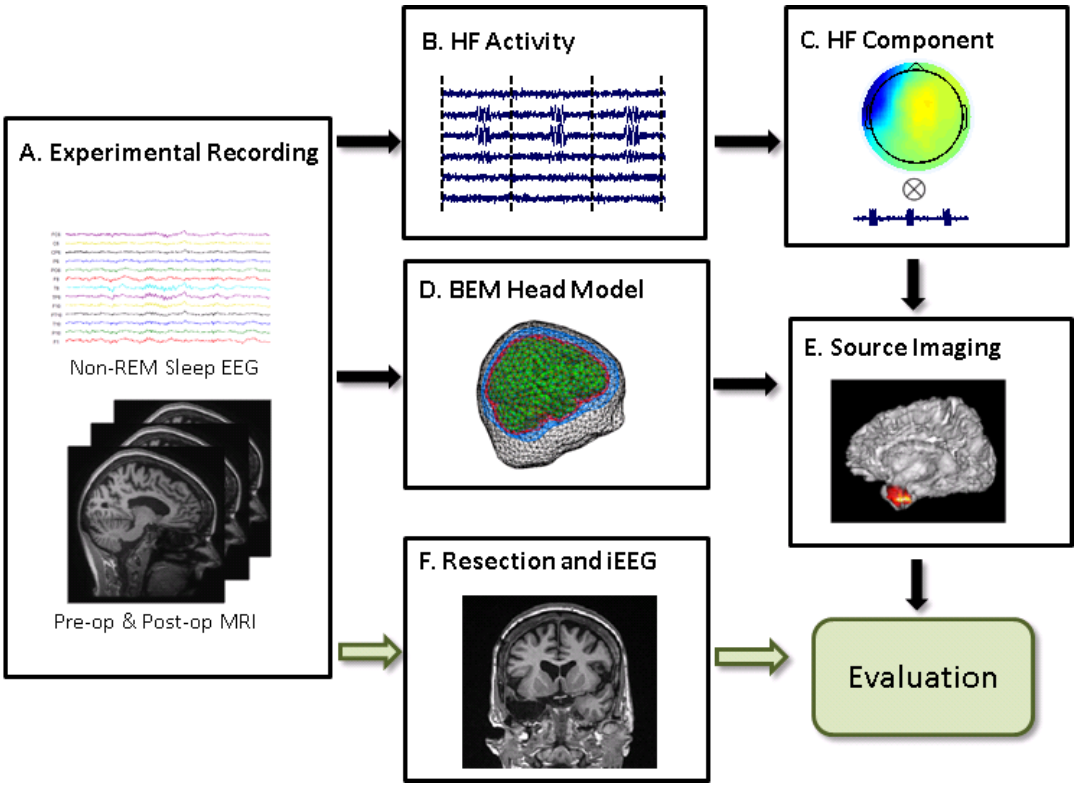

Fig. 5.1 Illustration diagram and study design of imaging high frequency (HF) activity. A: Experimental recording including non-REM sleep scalp EEG recording, pre-operative and post-operative MRI scans. B: Concatenated high frequency activity. C: Independent component according to the HF activity. D: Patient-specific boundary element head model. E: Source imaging of the HF activity. F: Surgical resection and intracranial recording of the patient.

In the present study, we utilized the noninvasive EEG source imaging approach to image the sources of HF activity recorded by the scalp EEG. HF activity was obtained from non-REM sleep stage of focal epilepsy patients and independent component analysis was used to extract the HF components for source imaging. The estimated sources for HF activity were then quantitatively compared with the surgically resected region and intracranial recordings of the patients.

5.2 Methods

5.2.1 High frequency source imaging

The high frequency source imaging (HFSI) approach (Lu et al., 2014) consists of concatenating the scalp recorded HF activity and imaging the high frequency components using the EEG source imaging. The scalp HF activity was obtained by reviewing the interictal data of the non-REM sleep EEG recording. The EEG data were high-pass filtered at 30Hz and the HF activity was identified as the activity with at least 3 consecutive oscillations.

The scalp EEG can be represented by modeling the brain electrical sources and the volume conduction effects. The general problem can be written in Equation (5.1).

$$\Phi = A(R, Q)\, S \tag{5.1}$$

The Nm-by-Nt matrix Φ is the electrical potential measured on the scalp, the Nm-by-3Ns matrix $A(R, Q)$ is the transfer matrix (or lead-field matrix), the Ns-by-1 vector R is the location of sources, the Ns-by-3 matrix Q is the orientation of sources, and the Ns-by-3Nt matrix S is the activity of brain sources. Nm is the number of EEG measurement on the scalp, Nt is the number of recorded samples in EEG, and Ns is the dimension of EEG source locations in source domain. The brain sources are modeled as the dipolar current sources located in the 3D brain and the transfer matrix is calculated from the boundary element method (BEM) head model (Hämäläinen and Sarvas 1989; He et al., 1987).

Since the HF activities are small oscillations and they cannot be averaged, independent component analysis (ICA) was utilized to extract the HF activity. The

spatial-temporal EEG activity can be represented by multiple independent components using ICA as in Equation (5.2) (Delorme and Makeig 2004; Yang et al., 2010; Yang et al., 2011).

$$\Phi = WMT = \sum_{i=1}^{N_C} w_i M_i T_i \tag{5.2}$$

where Φ is the recorded scalp EEG, N_C is the number of independent components, w_i is the i^{th} weighting element, M_i and T_i represent the spatial map and temporal activation of i^{th} component, respectively. Each component stands for an independent brain activity with spatial map and temporal activation. The components corresponding to the HF activity can be selected according to the repetitive appearance of HF activity in the component temporal activation. The brain source could then be estimated by solving the inverse problem of the spatial maps of HF components (Yang et al., 2011). Specifically, the source reconstruction for each HF component $\hat{S}_i$ will be obtained from its spatial map M_i, and the overall brain source S could then be obtained by combining the HF component sources in the source domain as $\sum_{i=1}^{N_S} w_i \hat{S}_i \hat{T}_i$, where $\hat{S}_i$ is the source of i^{th} HF component and $\hat{T}_i$ is the HF activity of i^{th} component. The estimated source S is thus the integrated result of all the identified HF component sources and it is the same as the individual component source when there is only one identified HF component. Varieties of source models and source imaging methods can be applied to solve the above inverse problem, and here we utilized the distributed current density source model and sLORETA weighted minimum norm estimation (SWARM) to estimate the brain sources

(Wagner et al., 2007). The patient-specific BEM head models were built from the pre-operative structural MR images of the patients. The volume conduction head modeling included three layers (scalp, skull and brain) and their conductivity values were set as 0.33 S/m, 0.0165 S/m and 0.33 S/m, respectively (Lai et al., 2005; Zhang et al., 2006).

5.2.2 Computer simulation of imaging high frequency activity

A series of computer simulations were performed to study the feasibility of imaging HF activity from the scalp EEG. Dipolar sources were simulated in the cortical structures and the simulated dipoles had random orientations. A standard head volume conduction model, built from MRI images of a human subject, was used to compute the forward problem and the scalp EEG with 76 channels were generated according to the source waveforms. Gaussian white noise was added to the scalp EEG signals to simulate noise contaminated measurements. In order to simulate the noisy conditions in EEG, the generated HF activity on scalp EEG is only slightly larger than the added noise in the EEG channels. We defined the signal-to-noise ratio (SNR) as the root-mean-square amplitude ratio of the signal and noise in the channel, which has the most dominant HF activity. A thousand trials with mean SNR 1.32 and standard deviation 0.39 were simulated to investigate the feasibility of studying HF activity. The HF activity of dipolar sources was simulated as the sinusoidal oscillation with the frequency at 40 Hz and the duration of the activity was set as 100 milliseconds. Background activity with 400 milliseconds in length was also simulated in addition to the HF activity, which leads to 500 milliseconds data for each data segment. Twenty data segments (10 seconds in total) were generated for each simulated dipolar source and the HF activity together with

background activity was used to estimate the source location and source orientation. Localization error (LE) was used to assess the source localization performance by calculating the distance between the location of maximal estimated source and the location of simulated target source. The computer simulation was carried out in 1000 trials and each trial consisted of a dipolar source with random location and orientation.

Table 5.1 Clinical information for the patients.

ID	Age at onset	Sex	Age	Structural MRI	Surgery	Interictal EEG	Number of HF activity	Outcome	Follow-up
1	22	M	26	Normal	Right temporal lobectomy	Frequent right temporal epileptiform activity	26	ILAE-1	36 mo
2	12	F	53	Left mesial temporal sclerosis	Left temporal lobectomy	Infrequent left temporal epileptiform discharges	13	ILAE-1	18 mo
3	22	F	33	Abnormal bilateral hippocampus	Right temporal lobectomy	Frequent right temporal spikes and sharp waves	20	ILAE-1	14 mo
4	7	F	25	Normal	Left parietal focal resection	Frequent left centro-temporo-parietal spikes	29	ILAE-1	17 mo
5	14	F	26	Normal	N/A	Frequent left temporal spike and sharp waves	20	N/A	N/A

5.2.3 Patient Data Acquisition and Analysis Protocol

The schematic diagram of patient data study is shown in Fig. 5.1. Five medically intractable focal epilepsy patients were studied and the study protocol was approved by the Institutional Review Boards of the University of Minnesota and the Mayo Clinic. Four patients underwent resective surgery (not spare procedure) and they had surgical outcome follow-up one year after the surgery. Two patients had intracranial recordings available and the seizure onset zones (SOZs) were identified for the patients by experienced epileptologists. All the patients had pre-operative long term EEG monitoring and pre-operative structural magnetic resonance imaging (MRI) scans. The clinical information of the patients is shown in Table 5.1.

The pre-operative scalp EEG was recorded in the long term video monitoring system with 76 electrodes placed according to the modified international 10-10 montage. The EEG data were filtered with a low-pass filter at 200 Hz and sampled at 500 Hz. The non-REM sleep EEG was then high-pass filtered above 30 Hz and displayed at expanded time-scale to mark the HF activity (Andrade-Valenca et al., 2011). The EEG segments containing HF activity were then concatenated together for independent component analysis. The pre-operative and post-operative MRI images (voxel size: 0.9375* 0.9375* 1.0 mm3) of the patients were acquired from a 1.5 Tesla or 3 Tesla GE Signa scanner (General Electric Medical Systems, Milwaukee, WI).

The source imaging results of high frequency activity were compared with the results of interictal spikes. The spikes were identified as these brief interictal discharges that had abrupt polarity changes from the background EEG. The dominant interictal spikes with similar morphology and topography were selected from each of the studied patients. The number of studied interictal spikes was the same as the number of studied HF activity and the interictal spikes were averaged according to their global field power (GFP) peak for further analysis. The source analysis of the interictal spikes was then performed by solving the inverse problem at the peak timing of the averaged spikes. Same as in estimating the HF activity sources, the SWARM source reconstruction algorithm was utilized to estimate the sources of interictal spikes.

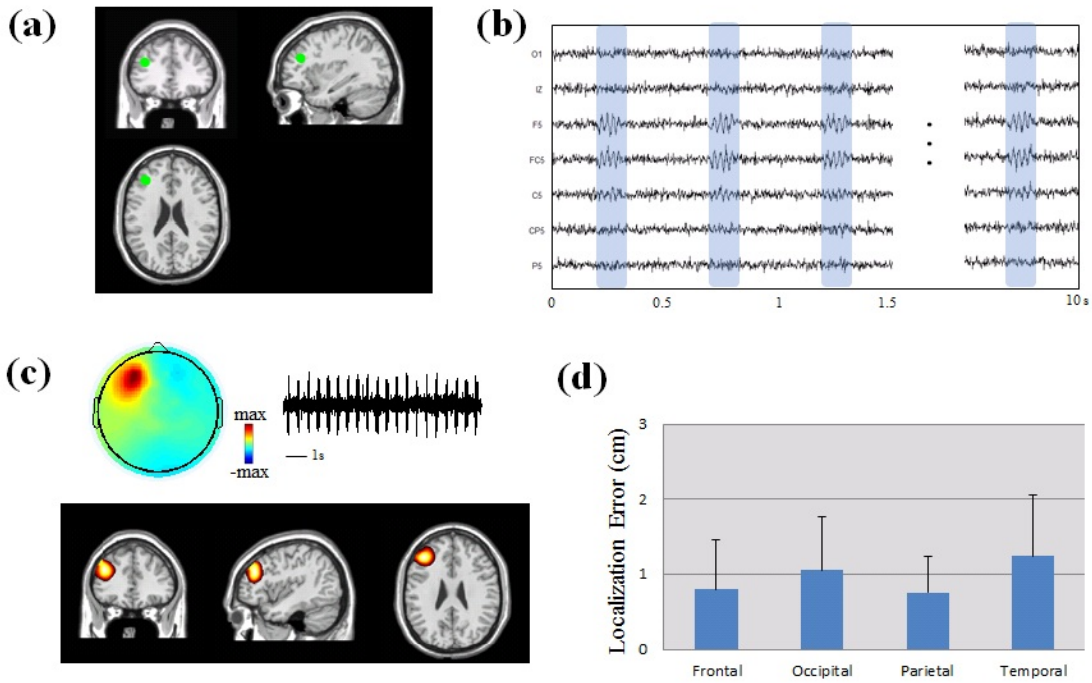

Fig. 5.2 Computer simulation of HF activity in a standard head volume conduction model. (a) Location of one simulated dipole source without extent in frontal lobe. (b) Scalp EEG traces generated from the simulated source. (c) Estimated sources and independent component of the HF activity. (d) Localization error (LE) of computer simulation in 1000 trials. The simulated dipoles are categorized in four groups according to the dipole locations (Frontal, Occipital, Parietal and Temporal groups).

5.2.4 Evaluation of imaging results in patients

The estimated sources for HF activity in patients were evaluated by comparing with the surgical resection and intracranial recordings in the same patients. The source location of HF activity was obtained by finding the strength maximum of the estimated source distribution. The surgically resected area was segmented from the post-operative MRI images of the patients. The SOZ was determined from the intracranial recording. Four patients had surgical resection and all of them were rendered seizure free within at least one year follow-up after the surgery. The localization error, which was defined as the distance from the maximal estimated EEG source to the border of surgically resected

regions or to the SOZ of the intracranial recording, was used to quantify the performance of HF source imaging in the epilepsy patients. Two patients had intracranial recording available, and the estimated sources were compared with the seizure onset zone that was marked on the intracranial recording electrodes.

5.3 Results

5.3.1 Computer simulation

The computer simulation results of imaging HF activity are shown in Fig. 5.2. One thousand trials were simulated and each trial included a dipolar source with random location and orientation located in the cortex. Fig. 5.2a shows the simulation settings of one simulated dipolar source. The location of the dipolar source is highlighted with the green dot and it is located in the left frontal lobe. Fig. 5.2b shows the simulated scalp EEG from the dipolar source based on the forward computation of the standard head modeling. Fig. 5.2c shows the source imaging results and the independent components of the high frequency activity. The estimated source is in the left frontal lobe and it is co-localized with the simulated source in frontal head region. The source imaging results from the 1000 trials are shown in Fig. 5.2d. The localization error is used to evaluate the performance in the computer simulation. The simulated trials are categorized into four groups (frontal, occipital, parietal and temporal groups) according to the locations of simulated dipoles. The results show that the mean localization errors are around 1 cm for all the groups with the smaller localization errors in frontal and parietal groups.

5.3.2 Imaging the high frequency activity

Patient 1 was a medically intractable patient with right temporal lobe epilepsy and the imaging results in the patient are shown in Fig. 5.3. Fig. 5.3a displays the wide-band raw EEG activity (left panel) and high-pass filtered EEG (right panel). The non-REM sleep EEG showed interictal spikes in the right hemisphere. Fig. 5.3b shows the independent

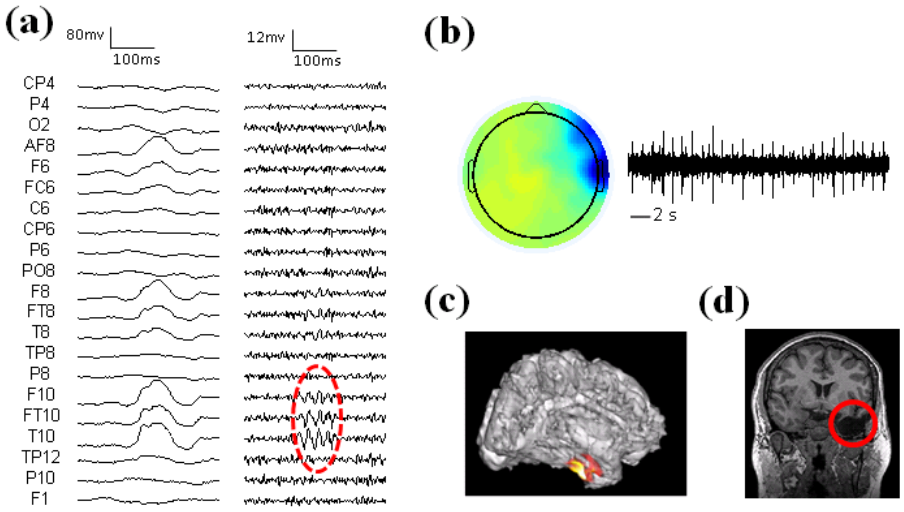

Fig. 5.3 Results in Patient 1. (a) Left: Raw EEG; Right: High-pass filtered EEG above 30 Hz. HF activity is marked with red circle. (b) Spatial map and temporal activation of one HF component. (c) Source imaging results of HF activity. (d) Surgical resection is highlighted in red.

component corresponding to the HF activity. The time activation of the component shows repetitive HF activity and the spatial map indicates that the activity is in the right temporal region. The source imaging result of the HF activity is displayed together with the cortex of the patient in Fig. 5.3c. This patient had the right temporal lobectomy and the resected brain region is highlighted with the red circle in Fig. 5.3d. The maximum of the estimated source is located in the right temporal lobe, which is concordant with the

surgical resection of the patient.

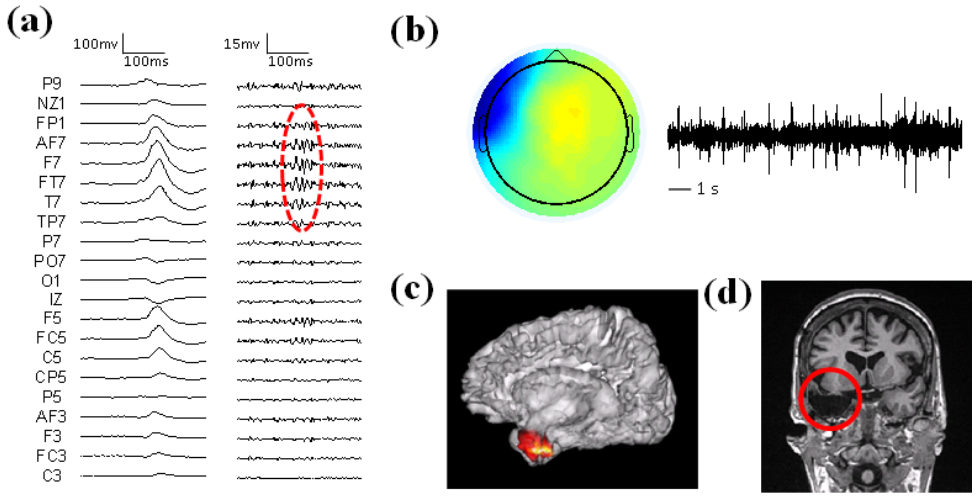

Fig. 5.4 Results in Patient 2. (a) Left: Raw EEG; Right: High-pass filtered EEG above 30 Hz. HF activity is marked with red circle. (b) Spatial map and temporal activation of one HF component. (c) Source imaging results of HF activity. (d) Surgical resection is highlighted in red.

The imaging results of Patient 2 are shown in Fig. 5.4. This patient had left temporal lobe epilepsy and was 33 years old during the epilepsy treatment. The non-REM sleep raw EEG show spikes in the left hemisphere and the high-pass filtered EEG show high frequency activity in left temporal head regions (Fig. 5.4a). Fig. 5.4b shows the independent component of the HF activity, which has repetitive HF time course and the spatial map is focused in left temporal region. The source imaging result of the HF activity is shown in Fig. 5.4c and the source maximum is in the left temporal lobe of the patient. This patient had left temporal lobectomy as demonstrated in Fig. 5.4d.

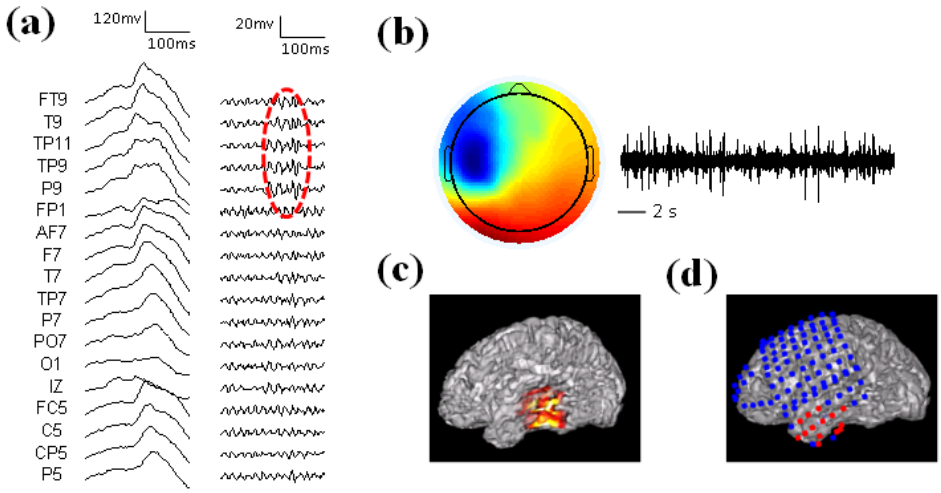

Fig. 5.5 Results in Patient 5. (a) Left: Raw EEG; Right: High-pass filtered EEG above 30 Hz. HF activity is marked with red circle. (b) Spatial map and temporal activation of one HF component. (c) Source imaging results of HF activity. (d) Seizure onset zone of intracranial recording is highlighted with red dots.

Patient 5 was a 26-year-old female epilepsy patient with left temporal seizures. The non-REM sleep EEG shows interictal spikes and the high-pass filtered EEG shows high frequency activity in the left hemisphere (Fig. 5.5a). Fig. 5.5b shows the independent component of the HF activity, which has repetitive HF time course and the spatial map is focused in left temporal region. The source imaging result of the patient is in the left temporal lobe region and it is concordant with the seizure onset zone of intracranial recording as shown in Fig. 5.5d.

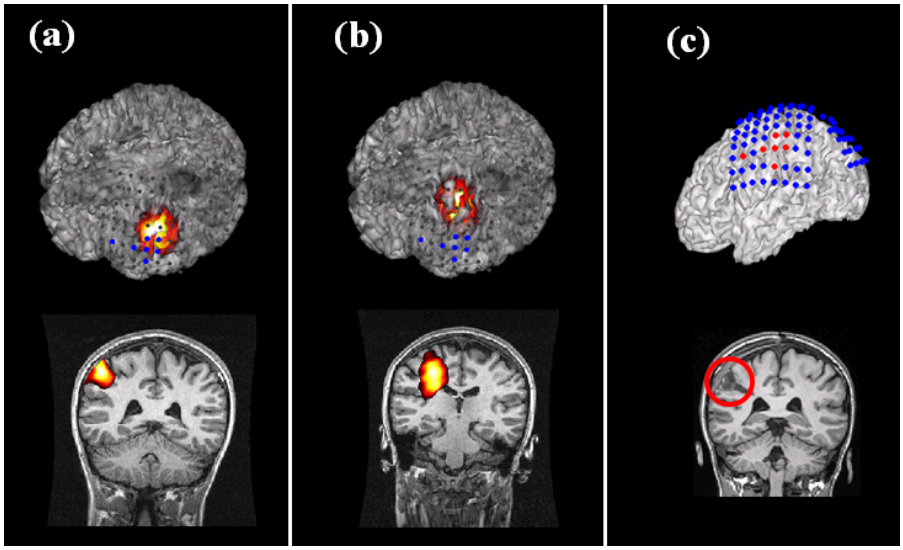

Fig. 5.6 Comparison between source imaging of HF activity and interictal spike in Patient 4. (a) Source imaging results of HF activity. (b) Source imaging results of interictal spike. (c) Intracranial recording and surgical resection.

The source imaging results of all five patients are summarized in Fig. 5.7. The estimated sources of the patients were evaluated with surgical resection and intracranial recordings. In three out of the four patients with surgical treatment, the estimated source maxima were located inside the surgically resected regions. The estimated source in the remaining patient was close to the resection boundary. In the two patients with intracranial recording available, the estimated sources were overlapped with the SOZ determined from intracranial recordings. In addition to the source analysis of high frequency activity, we also analyzed the sources of interictal spikes in the same group of studied patients.

5.3.3 High frequency activity and interictal spikes

The source imaging results of high frequency activity were compared with the results of interictal spikes. Fig. 5.6 shows the source imaging results of HF activity and interictal

spike in Patient 4. Fig. 5.6a shows the results of HF activity as displayed with intracranial recording electrodes and pre-operative MRI images of the patient. The imaged source of HF activity is located in the left parietal lobe, and it is concordant with the SOZ of intracranial recording and the surgical resection as highlighted in Fig. 5.6c. The source imaging result from conventional interictal EEG spike is shown in Fig. 5.6b. The spike result is in medial area and it is slightly shifted from the SOZ as determined from intracranial EEG and surgical resection. This result suggests that the HF activity source imaging could more accurately image the location of epileptogenic sources than the spike analysis. The localization of HF activity and spikes are also quantitatively compared in the four patients (Patient 1, Patient 2, Patient 3, and Patient 4) who had surgical resection available and in the two patients (Patient 4 and Patient 5) who had intracranial recording available. The averaged localization error to the surgical resection is 0.25 cm in HF activity and 0.53 cm in the spike results (Fig. 5.7a). The averaged localization error to the seizure onset zone of intracranial recording is 1.2 cm in HF activity while it is over 2 cm in the spike results (Fig. 5.7b). The above results show that the HF activity is more effective in imaging the epileptogenic zone than the interictal spike as compared with the SOZ of intracranial recording and the surgical resection.

5.4 Discussion

In the present study, we imaged the brain sources of scalp high frequency activity in five medically intractable focal epilepsy patients. The estimated brain sources of HF activity were concordant with the locations of surgical resection and SOZ determined from intracranial recordings. The imaging of HF activity also showed improved performance in localizing epileptogenic zone as compared with the traditional source analysis of interictal spikes. This study demonstrates that source imaging of the scalp HF activity may represent a new noninvasive way of identifying the epileptogenic zone for

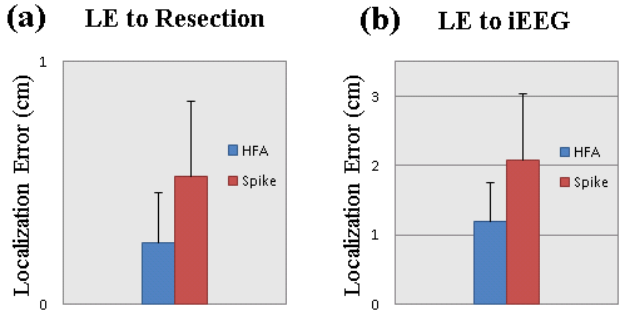

Fig. 5.7 Localization error between source imaging of HF activity and spike (a) Localization error comparing with surgical resection. (b) Localization error comparing with SOZ of intracranial recording.

the pre-surgical planning of epilepsy treatment.

High frequency brain oscillations appear to be an effective biomarker of delineating the pathological epileptogenic zone from the normal brain regions (Jacobs et al., 2012; Worrell and Gotman 2011). Studies have shown that brain areas with high frequency (HF) activity greatly overlapped with the SOZ and the HF activity is more likely to occur within the SOZ than in other regions. Retrospective studies also showed that there is a strong association between seizure-free outcome and removal of HF generating regions during the surgical treatment (Ochi et al., 2007). Another reason to suggest HF activity as

an effective biomarker is that HF activity is useful in revealing epileptogenic zone rather than indicating the non-specific pathological MRI lesions (Jacobs et al., 2009; Staba et al., 2007). This property ensures that HF activity could be used to identify the epileptogenic zone in MRI-negative patients and to exclude the non-epileptic MRI abnormalities in patients with multiple lesions. Since the report of successful recording of HF brain oscillation in epilepsy patients, various studies have demonstrated the usefulness of HF activity in the pre-surgical planning of epilepsy treatment. Recent studies of epilepsy patients also reported the recording of HF brain oscillations in scalp EEGs, which suggested the importance of noninvasive study on the HF activity for potential clinical application (Andrade-Valenca et al., 2011; Kobayashi et al., 2011).

EEG/MEG source imaging has been previously used to analyze the functioning brain response in normal subjects and to study the pathological brain activity in epilepsy patients (Darvas et al., 2004; He and Ding 2013; Kaiboriboon et al., 2010; Lai et al., 2011; Lu et al., 2012b; Plummer et al., 2007; Wang et al., 2012b). The advancement in source imaging techniques has enabled the feasibility of studying the underlying brain sources from the noninvasive recording of electromagnetic activity. Scanning methods such as multiple signal classification and spatial filtering approaches has been utilized to probe the brain electrical sources from noninvasive recordings (Ding et al., 2007b; Leahy et al., 1998; Lu et al., 2012b; Mosher and Leahy 1999; Van Veen et al., 1997; Xu et al., 2004). Source imaging methods for current density models were also developed to image the active brain sources with certain distribution (Dale et al., 2000; Hämäläinen and Ilmoniemi 1984; Pascual-Marqui 2002). Previous source imaging studies of epilepsy

patients have been mainly focused on the spikes during the interictal periods. Considering the effectiveness of high frequency brain activity in characterizing the epileptogenic zone, it remains important to study the cortical brain sources corresponding to the scalp high frequency activity. In this study, the scalp high frequency activity was successfully imaged and the estimated brain sources were concordant with the seizure onset zone as referenced from surgical resection and intracranial recording of the patients.

An important issue in the EEG source analysis of epilepsy patients is to record the desired epileptic events and to image the events with high spatial and temporal resolution. In this study, the scalp electrophysiological activity of epilepsy patients was recorded using the long-term video EEG monitoring system. The long-term monitoring enabled the recording of EEG activity during the sleep stage of the patients while the head moving artifacts could be minimized (Andrade-Valenca et al., 2011). The sampling frequency of the recording was set at 500 Hz to capture the high frequency activity above 30 Hz of the scalp EEG. Studies have shown that the source localization accuracy could be improved by utilizing the dense-array EEG recording system (Lantz et al., 2003; Lu et al., 2012b). High-density EEG recording with 76 electrodes were utilized in this study to overcome the limited spatial sampling of 19 or 21 channels as in the routine clinical settings. The patient-specific realistic geometric BEM head modeling was used in the study to further minimize the localization error that is caused by the inaccuracy of volume conduction modeling (Hämäläinen and Sarvas 1989; He et al., 1987; Wang et al., 2010). In the present study, the scalp recorded HF activity was processed with independent component analysis to extract the HF components. The number of selected ICs varies among the

patients and it ranges from one to three components in the studied patients. When more than one IC is identified, the HF sources for each of the identified IC are estimated and the source results are obtained by combining the component sources in the source domain. HF activity was obtained during the non-REM sleep EEG of the patients in order to minimize the recording noise. Future studies incorporating advance techniques to study the HF activity in other routine EEG recordings such as during less frequent spikes or during ictal events may be necessary to further investigate the high frequency activity in more noisy conditions and improve the clinical application. All patients in the current study had partial epilepsy with single epileptic focus, and studies including more patients and more complicated patients such as patients with multiple foci would be beneficial to expand the analysis in more general epilepsy cases. Future studies comparing the scalp HF activity with invasive high frequency activity may also be necessary to further understand the epileptic activity and enhance the application.

Despite the great efforts of many studies in imaging the epileptogenic zone, it remains a significant challenge to accurately identify the abnormal brain regions for a successful surgical treatment. Various imaging modalities have been used to image the epileptogenic zone in medically intractable epilepsy patients. Single-photon emission computed tomography (SPECT) and positron emission tomography (PET) have been applied to study the perfusion and metabolism of epileptic brain. Functional MRI (fMRI) was also utilized to study the BOLD response under resting state of epilepsy patients. Recent studies have shown that multimodal neuroimaging combining the EEG and fMRI could achieve improved performance by integrating the high temporal resolution of EEG and

high spatial resolution of fMRI (Babiloni et al., 2005; He and Liu 2008; Liu and He 2008; Pittau et al., 2011; Vulliemoz et al., 2011; Yang et al., 2010). Studies also revealed the strong spatial correlation between the task-related fMRI activation and gamma activity of intracranial EEG in the same epilepsy patients (Lachaux et al., 2007). Advanced algorithms and techniques have been previously developed to help on the diagnosis and treatment of epilepsy (Collier et al., 2012; Conradsen et al., 2012; De Silva et al., 2012; Fukushima et al., 2012; Liu et al., 2013; Rana et al., 2012; Sun et al., 2012; Temko et al., 2012; Wang et al., 2012a; Wu et al., 2012a; Wu et al., 2012b; Yadav et al., 2012a; Yadav et al., 2012b). Future studies investigating the feasibility of integrating high frequency EEG activity and spontaneous fMRI is still necessary to further develop advanced multimodal neuroimaging techniques for the clinical application in epilepsy patient management.

In conclusion, we proposed the high frequency source imaging method to image the high frequency brain activity from scalp EEGs of epilepsy patients. A series of computer simulations have been performed to test the feasibility of imaging the dipolar sources with high frequency source activity. The proposed method has been evaluated in five medically intractable epilepsy patients and it successfully imaged the underlying sources of scalp high frequency activity as compared with the surgical resection and intracranial recording of the patients. The present study demonstrates, for the first time, the feasibility of noninvasively imaging scalp high frequency activity in the epilepsy patients. It also indicates its potential application as a novel noninvasive way of localizing the epileptogenic zone and in aiding the pre-surgical planning of epilepsy treatment.

Chapter 6 Noninvasive Imaging of the Source Extent from EEG

6.1 Introduction

Epilepsy is a chronic neurological disease that affects about 50 million people worldwide. Patients with epilepsy will have unpredictable and uncontrolled seizures, which greatly impact the quality of life of the patients. Epilepsy patients can be treated with antiepileptic drugs (AED), however, about 30% of the patients cannot have their seizures suppressed even after trying multiple antiepileptic medications. Many patients, with frequent seizures but resistant to the medications, are seeking the hope from resective surgery, which can eliminate the seizures and cure the epilepsy. The accurate estimation of source location and extent of epileptogenic zone is thus of great importance to provide a useful tool in aiding the pre-surgical planning of resective surgery.

The current gold standard of identifying the epileptogenic zone in clinic is using the intracranial recordings, such as cortical grid or depth electrodes. During the intracranial monitoring, the patients are generally required to undergo open-skull procedure and the recording electrodes will be implanted over the cortical surface or inserted into the brain tissue. The intracranial recordings will last for a few days and the electrophysiological data will be reviewed to identify the seizure onset zone (SOZ) for surgical resection. Considering the invasive nature of the intracranial monitoring and the high cost of performing such procedures, the intracranial recordings are only available in

This work was done together with Mr. Abbas Sohrabpour.

large epilepsy centers. In addition, the intracranial recordings have limited spatial coverage and only a limited portion of the brain can be covered with electrodes, due to the access constrains of open-skull procedure and the prevention of impairing normal brain function.

Electroencephalography (EEG) is the noninvasive recording of synchronized neuronal activity from human brain. Scalp EEG has high temporal resolution at millisecond scale and it has been widely used to study the normal brain function in healthy subjects and the pathological brain functional in diseased brain (Michel et al., 2004; He et al., 2011). EEG is routinely used in hospitals and clinics to help the diagnosis and monitoring of epilepsy. EEG source imaging has also been utilized to study the underlying brain sources of neuronal activity. Previous studies have shown the great usage of EEG source imaging approaches in localizing the sources of interictal activity and seizure activity of epilepsy patients (Wang et al., 2010; Lai et al., 2011; Lu et al., 2012, 2014; Yang et al., 2011).

Source localization approaches based on various principles and techniques have been developed to provide the estimation of EEG sources. Equivalent dipole model was proposed and used to solve the inverse problem and gave the estimation of a few isolated brain sources. Spatio-temporal approaches, such as beamforming, multiple signal classification (MUSIC), and first principle vectors (FINE), were also used to localize the source with great resolution (Mosher et al., 1992; Van Veen et al., 1997; Lu et al., 2012). Physiologically meaningful prior information, such as minimum source energy

assumption in minimum norm estimation (MNE) and maximized smoothness assumption in low resolution brain electromagnetic tomography (LORETA), were also used in the source imaging approach to give robust estimation of the source activity (Hämäläinen and Ilmoniemi, 1984; Pascual-Marqui et al., 2002). The aforementioned methods have shown great performance in localizing the functional brain activity; however, these methods were not specifically designed for estimating the source size and it is still challenging for the methods to provide accurate estimation of the source extent. It is also desirable to have source imaging method to image both the location and size of the brain activity, which is of great clinical importance in identifying the epileptogenic zone in epilepsy patients.

In this study, we developed an EEG source extent imaging approach which can image both the location and size of the EEG source. Innovative edge sparse estimation method and multi-resolution method were incorporated in the proposed imaging approach in order to give an accurate estimation of the source extent. The method was evaluated with a series of computer simulations and a group of epilepsy patient data. The results shows great concordance of the estimated source extent by comparing with the simulated source size or clinical identified epileptic brain size.

6.2 Method

6.2.1 EEG source extent imaging

We developed a novel approach to accurately estimate the source extent in epilepsy patients. Innovative edge sparse estimation method and multi-resolution method

were incorporated in the proposed imaging approach in order to give an accurate estimation of the source extent. The general problem of EEG source imaging can be expressed as

$$\Phi(t) = A(R)S(t) \tag{6.1}$$

where $\Phi(t)$ is the measured EEG potential on the scalp layer at time t, $A(R)$ is the lead-field matrix for source locations R, $S(t)$ is the source activity at time t. The forward equation is established to estimate the source locations R in the cortical source spaces that best fit the EEG signal. Once the lead-field matrix $A(R)$ is constructed, the source activity $S(t)$ can be estimated by solving the inverse problem. The general formulation of the inverse problem can be written as Equation (2).

$$\arg\min_{S} (\|\Phi - A * S\|_2 + \|\lambda * B * S\|_2) \tag{6.2}$$

where $\|\bullet\|_2$ is the Frobenius norm operator (L2 norm), λ is the regularization term, and B is the source weighting matrix for the inverse solution. Varieties of source models and source imaging methods can be applied to solve the above inverse problem. For instance, if B is the identify matrix, the solution is the regular minimum norm estimation (MNE). The solution is low resolution brain electromagnetic tomography (LORETA) when the Laplacian matrix is used to solve the problem. However, the source imaging results from L2-norm type methods are generally over-smoothed. By performing the sparse L1 norm on the inverse problem, we can obtain some spare source of the EEG

activity. Furthermore, if we apply the sparse L1 norm on the spatial gradient of the source, we are able to reconstruct the signal that only has limited spatial jump, i.e. the edges of the source distribution. The new optimization problem becomes following

$$\arg\min_{s} \left(\left\| \Phi - A * S \right\|_2 + \left\| \lambda * V * S \right\|_1 \right) \tag{6.3}$$

where $\left\| \bullet \right\|_1$ is the L1 norm for spare solution, V is the discrete gradient operator. The reason for using L1 norm in (6.3) is that using L0 norm, which is basically counting the non-zero elements of a vector, would make the problem non-convex and difficult to solve. However, it is well-known that interchanging L0 norm with L1 norm will give solutions that are close to the desired solutions (Donoho, 2004). As the optimization problem formulated in (6.3) is a convex optimization problem, solving (6.3) is easy due to the abundance of developed techniques in convex optimization. Thus, solving such seemingly complex optimization problem will not be a difficulty.

In addition to the edge sparse estimation method, we also propose a multi-resolution method to refine the extent estimation in a two-step approach. Edge sparse method is firstly applied on the whole source space in order to get an initial estimation of the source distribution. Another edge sparse reconstruction based on the initial estimation is then performed to obtain a refined estimation of the source extent. If λ is large enough, the underlying source will be overestimated. We can use this to weight the optimization problem. Intuitively, the dipoles located outside the initial estimate can be penalized more by assigning a larger weight to them, while the dipoles located within the initial estimate

can be assigned a smaller weight and thus penalized less. Thus a second optimization problem formulated as follows can be used

$$\arg\min_{s} \left(\left\| \Phi - A * S \right\|_2 + \left\| \lambda * VW_1 * S \right\|_1 + \left\| \gamma * W_2 * S \right\|_1 \right) \tag{6.4}$$

where W_1 and W_2 are diagonal weighting matrices derived from the initial estimate which is derived from solving (6.3). The reason the second term is added, is to guarantee a zero background. A slow alternating background may not adversely affect the first and second term in (6.4) so the addition of the third term damps such oscillations. The two optimization problems described in (6.3) and (6.4) can be easily solved. The proposed method works well, since it not only considers the inherent redundancy of the underlying source, i.e. edge-sparsity, but also increases its precision by weighting out improbable dipoles in a data-driven approach. The efficient and fairly mature mathematical techniques of solving the proposed optimization problem and the excellent performance of the proposed method make it a perfect candidate for clinical applications. The proposed optimization method can be applied to interictal spikes to find the extent of the SOZ.

6.2.2 Computer simulation

In order to systematically test the proposed extent imaging method, a series of computer simulations were performed. A realistic geometry cortex was formed from the MR Images of a patient. 100 random locations were selected from this cortex. At each location a source with different extent was created, i.e. a circular source with

radius 10mm, 20mm and 30mm. Solving the forward problem, using a realistic head BEM model composing of three layers which modeled scalp, skull an brain with conductivities of 0.33 S/m, 0.0165 S/m and 0.33 S/m, the scalp potential was formed (in a 128 channel EEG recording setting). White Gaussian noise was added to the simulated scalp potential and the inverse solution under different signal-to-noise ratio (SNR) levels was obtained using the proposed sparse method.

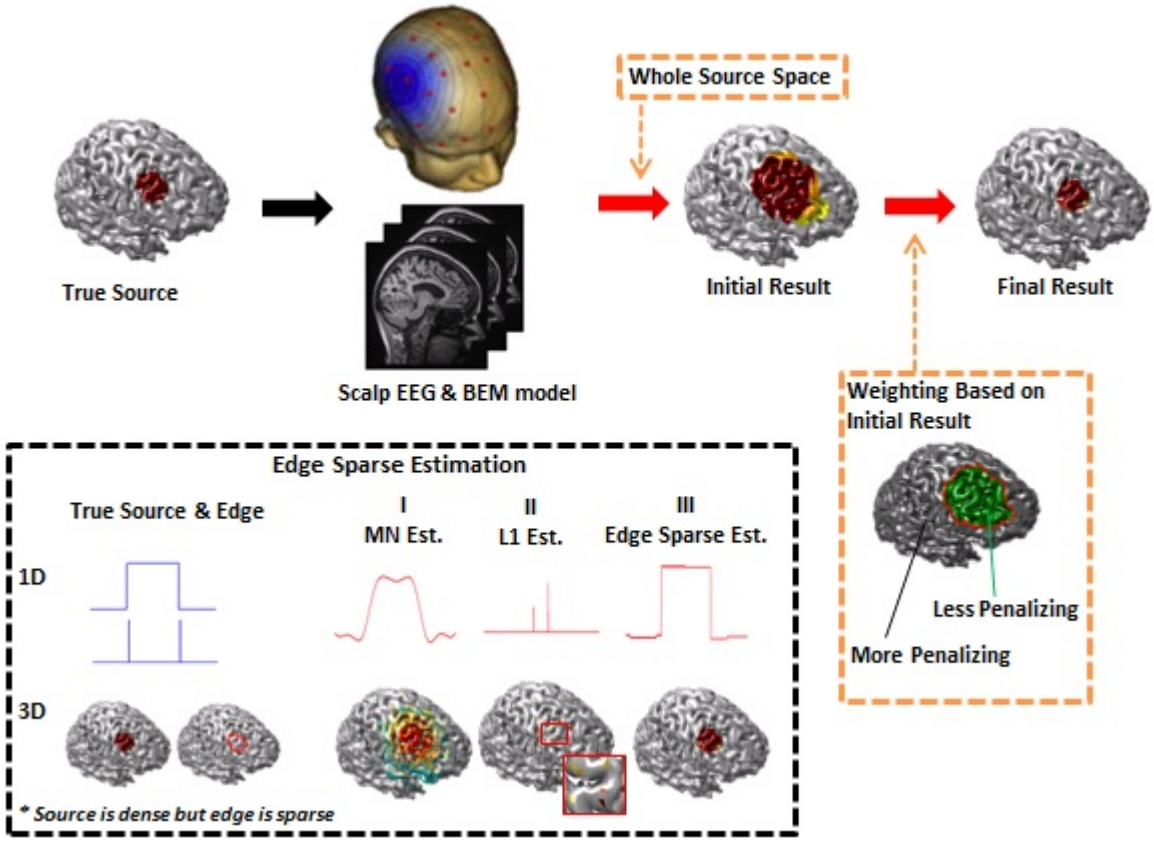

Fig. 6.1 Schematic diagram of the proposed method. Two novel strategies (edge sparse estimation and multi-resolution method) were proposed to accurately estimate the source extent.

The schematic diagram of the method can be found in Fig. 6.1. The edge sparse estimation is based on the prior information that source is densely distributed but the

source edge is sparse. The source extent can thus be obtained by adding the edge-sparse term into the source optimization solution. The multi-resolution method is based on a two-step approach. The first step is to use the edge sparse method to get the initial source estimation from the whole source space. The initial source solution is smooth and overestimates the extent. The second step is then performed to more accurately estimate the source extent by applying less penalize in initial active sources and more penalize in initial non-active sources.

6.2.3 Patients and data analysis

The noninvasive scalp EEG of five epilepsy patients was obtained during a clinical EEG recording system. The EEG signals were pre-processed with a band-pass filter (1-70Hz) and the sampling frequency is 500 Hz. The EEG data was obtained with 76 channels and the recording electrodes were set up according to the modified international 10-20 montage. The EEG data were reviewed to identify the interictal spikes of the patients. A total of five patients were analyzed using the source extent imaging approach. Pre-surgical structural magnetic resonance imaging (MRI) was acquired in all the patients. The MR images have the resolution of 0.9375 mm * 0.9375 mm * 1.0 mm and they were acquired from a 1.5 Tesla or 3 Tesla GE Signa scanner (General Electric Medical Systems, Milwaukee, WI). Patient-personalized realistic head model using boundary element method (BEM) was obtained from the MR images in Curry tools (Compumedics, Charlotte, NC).

6.2.4 Evaluation of source extent imaging

The source extent imaging results were quantitatively evaluated in the computer simulation and patient data analysis. In case of simulations, there are specific metrics that can be used to evaluate the obtained solution, as the true underlying source, i.e. the simulated source, is known in advance. Some examples that can be implemented are as follows. The localization error (LE) which is defined as the distance between the center of mass of the estimated and simulated source is one measure that shows the relative shift between the true and estimated source. Another one is the ratio of the estimated source area to the true simulated area, which shows how precise the estimate of the extent is. Another metric is the ration of the overlapping area between the true and estimated source divided by either the true source area or the estimated source area. One other metric would be the AUC, sensitivity and specificity which show how good the two distributions, i.e. the estimated and true underlying source, match.

The proposed EEG source extent imaging algorithm was also tested in real clinical data the five epilepsy patients. The studied patients suffered from frontal, temporal, or parietal partial epilepsy and their interictal spikes were analyzed to estimate their source extent. Four of the patients underwent surgery and were seizure free afterwards. Each patient had interictal spikes recorded during the EEG monitoring. The spikes were averaged and the proposed method was used to find the inverse solution at spike peak time. Three patients underwent invasive ECoG recording prior to surgery and the epileptologist marked seizure onset zone (SOZ). The ECoG electrode location was

extracted from CT images of the patients and compared with the obtained inverse solution.

6.3 Results

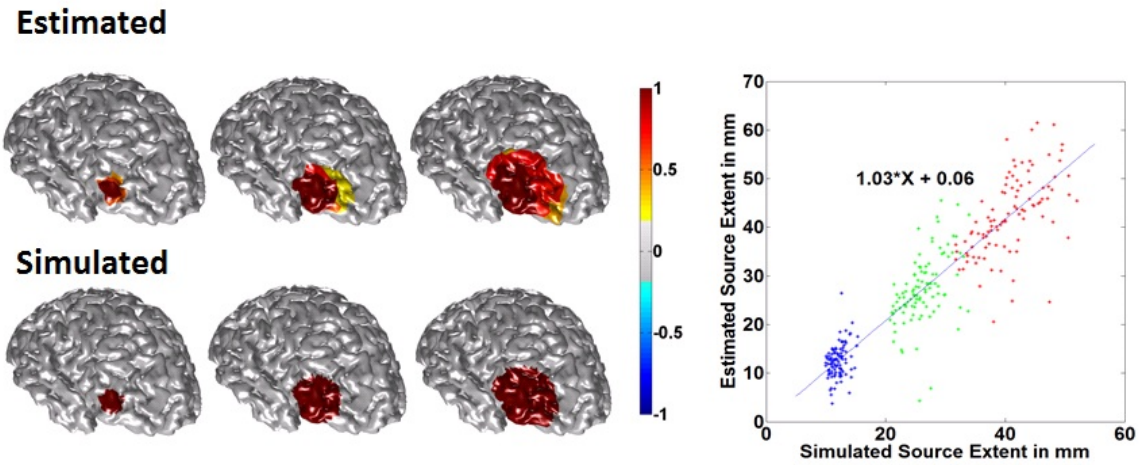

Fig. 6.2 Simulation results. In the left panel three different source sizes were simulated with extents of 10 mm, 20 mm and 30 mm (lower row). The extent of the estimated source is compared to that of the simulated source in the right panel in 100 simulations. The SNR is 20dB.

Computer simulations were performed to test the feasibility of the source extent imaging. Fig. 6.2 shows the results of different source sizes (with extents of 10 mm, 20 mm and 30 mm) when the simulated SNR level is 20dB, and the estimated results are consistent with the simulated sources. White Gaussian noise was added and the inverse was solved using the proposed method. The results are shown in the top row of left panel and the simulated sources are shown in the lower row of left panel. The same procedure was repeated for simulated random locations over the cortex. The extent of the estimated source in 100 simulations is compared to that of the simulated source in the right panel. A

linear relationship was observed between the simulated and estimated source size with the fitting slope as 1.03 and the fitting intercept as 0.06.

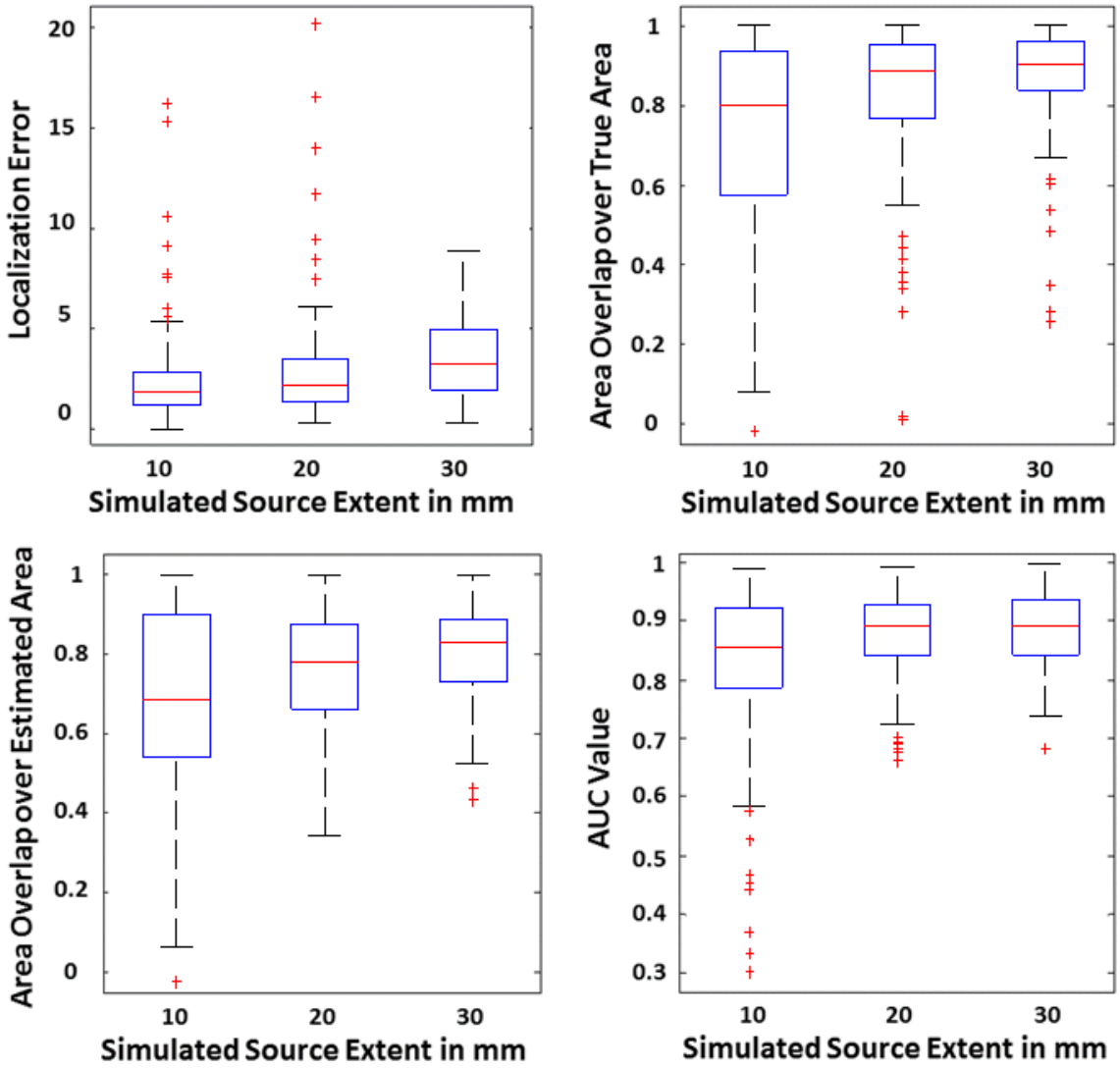

Fig. 6.3 Simulation statistics. The performance of the simulation study is quantified using the following measures, localization error, AUC and the ratio of the area of the overlap between the estimated and true source to either the area of the true source or the area of the

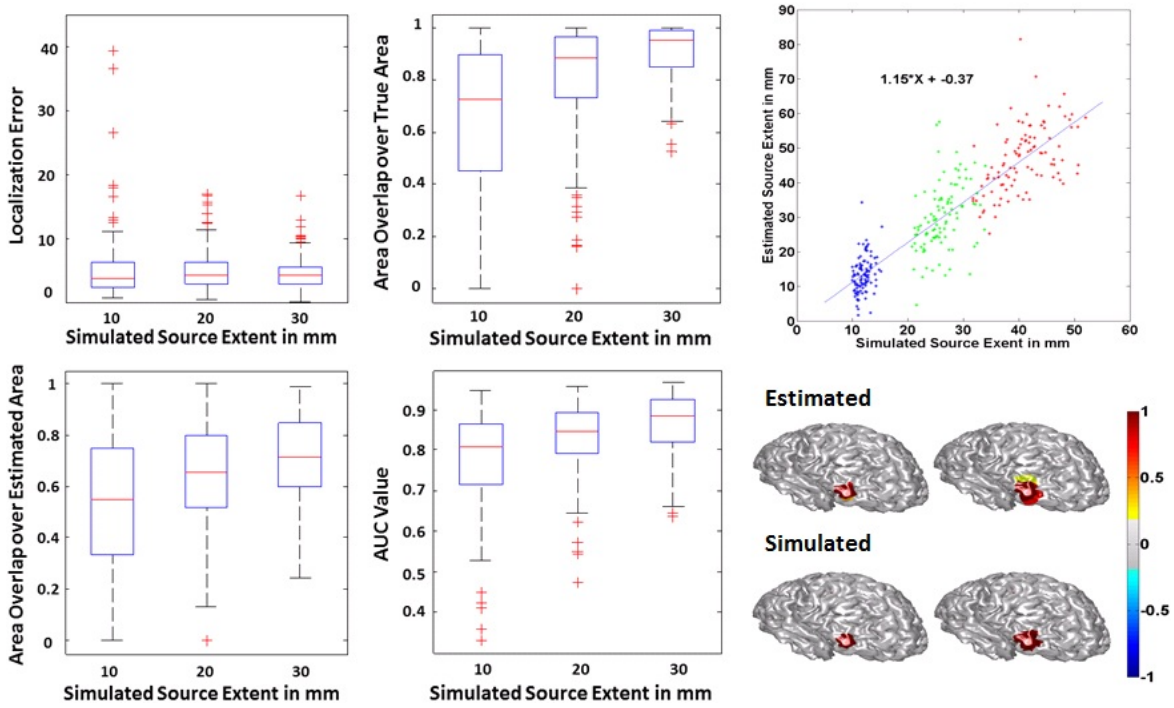

Fig. 6.4 Simulation statistics and performance of the simulation study when the SNR is 10dB. Results are quantified using the following measures, localization error, AUC and the ratio of the area of the overlap between the estimated and true source to either the area of the true source or the area of the estimated source. The statistics are shown in the left panel. In the right panel, the relation between the extent of the estimated and simulated source is delineated (top row). Two different source sizes namely, 10 mm and 15 mm, were simulated and the results are depicted in the right panel (bottom row).

Fig. 6.3 shows the statistical analysis of evaluating the computer simulation results. Different metrics, such as localization error, AUC, and volume overlapping were used to quantify the performance. It can be seen that the mean localization error is within 5 mm for all the three different simulated source sizes. The mean overlapping to the simulated source and estimated source are all above 70%. The mean AUC values for different source sizes are all above 0.8. All these results suggest that the method can accurately estimate the source size in computer simulation. Fig. 6.4 shows the extent

estimation when the simulated SNR is about 10dB and they also show the consistent results as compare with the simulated source.

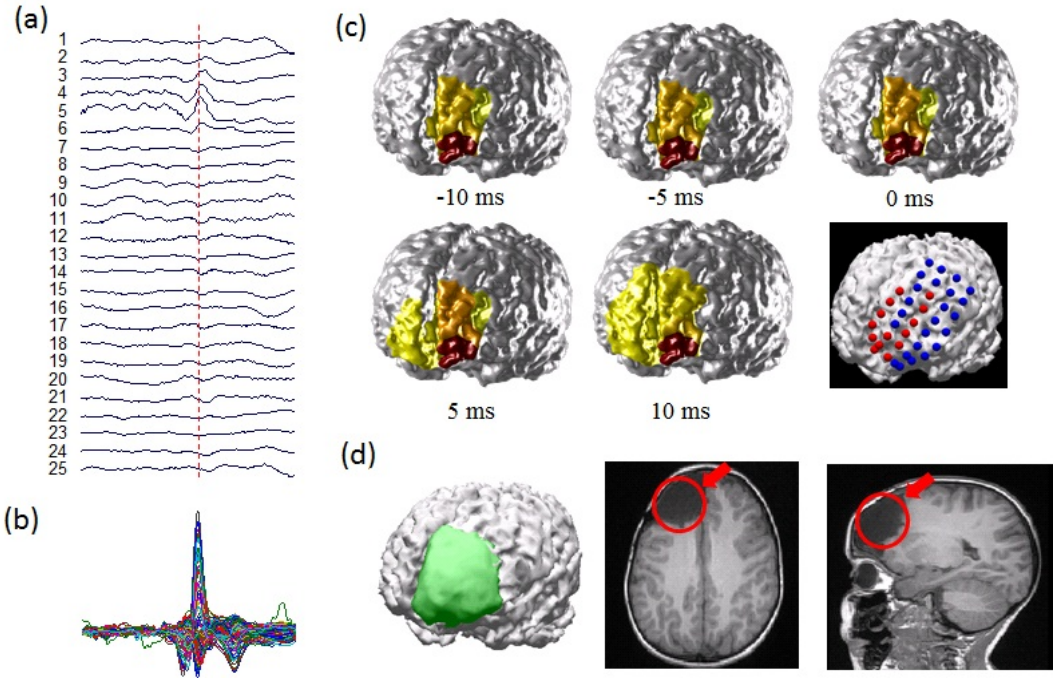

Fig. 6.5 Source extent estimation results in a patient with frontal epilepsy. (a) Scalp EEG wave of the interictal spike. (b) Butterfly plot of the spike waveform. (c) Estimation results of source extent at different latency of the interictal spike. Right subpanel shows the SOZ of the intracranial recordings. (d) Surgical resection of the patient.

Fig. 6.5 shows the extent estimation results in an epilepsy patient. This patient is a pediatric patient with frontal lobe epilepsy. This patient had frequency interictal spikes during the EEG recording. Fig. 6.5(a) shows an example interictal spike with the spike peak marked out with the vertical red line. Fig. 6.5(b) shows the butterfly display of the interictal spikes which shows a clear spike in the EEG signals. Fig. 6.5(c) shows the source extent imaging results in consecutive 20 millisecond time window centered at spike peak. The SOZ of the intracranial recording was marked in Fig. 6.5(c) and the surgical resection of the patient was marked in Fig. 6.5(d). It can be noticed that the

patient had left frontal resection and the estimated source extent is consistent with the clinically diagnosed SOZ.

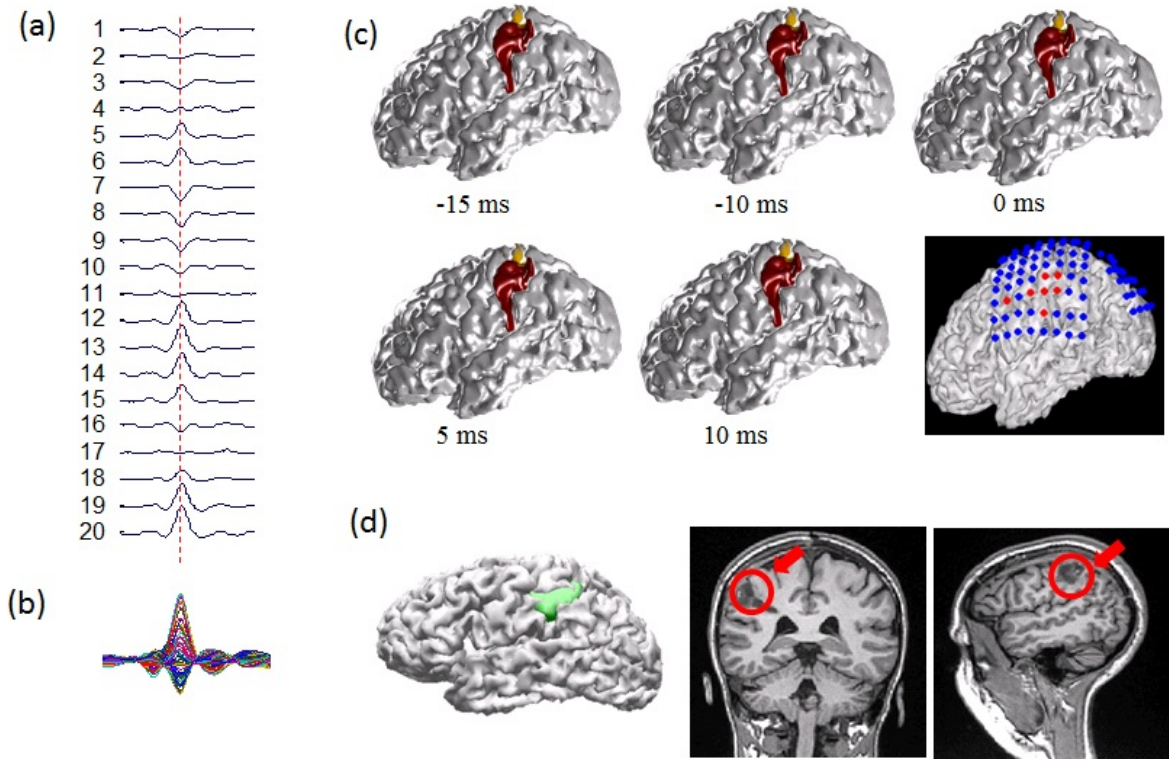

Fig. 6.6 Source extent estimation results in a patient with parietal epilepsy. (a) Scalp EEG wave of the interictal spike. (b) Butterfly plot of the spike waveform. (c) Estimation results of source extent at different latency of the interictal spike. Right subpanel shows the SOZ of the intracranial recordings. (d) Surgical resection of the patient.

Fig. 6.6 shows the extent estimation results in another epilepsy patient. This patient had medically intractable parietal lobe epilepsy. This patient had frequency interictal spikes during the EEG recording. Fig. 6.6(a) shows an example interictal spike with the spike peak marked out with the vertical red line. Fig. 6.6(b) shows the butterfly display of the interictal spikes which shows a clear spike in the EEG signals. Fig. 6.6(c) shows the source extent imaging results in consecutive 20 millisecond time window

centered at spike peak. The SOZ of the intracranial recording was marked in Fig. 6.6(c) and the surgical resection of the patient was marked in Fig. 6.6(d). It can be noticed that the patient had focal left parietal resection and the estimated source extent is consistent with the clinically diagnosed SOZ and the surgical resection.

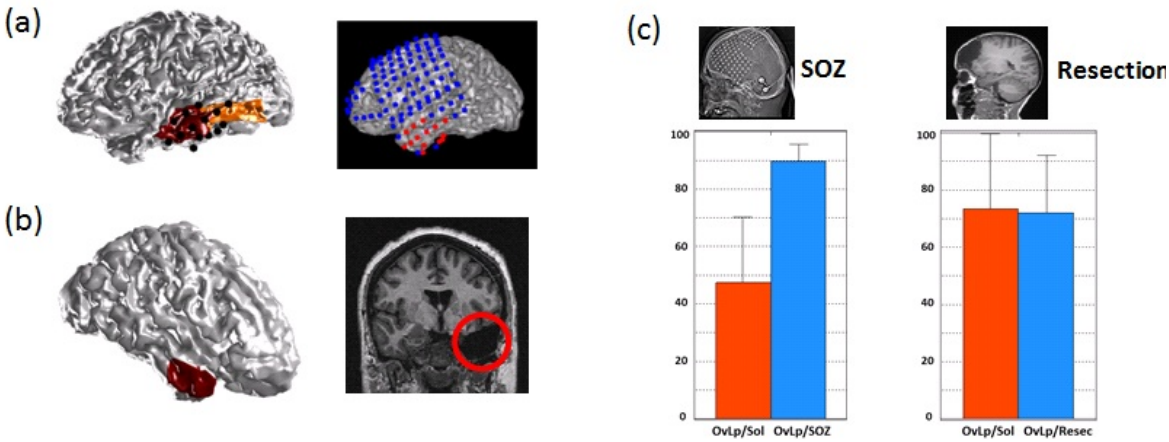

Fig. 6.7 Source extent estimation results in all patients. (a) Estimation results of source extent in a temporal epilepsy patients by comparing with SOZ of the intracranial recordings. (b) Estimation results of source extent in another temporal epilepsy patients by comparing with surgical resection. (c) Quantitative results of the source extent estimation by calculating the area overlapping of the estimated source with SOZ and resection.

Left panels of Fig. 6.7 show the extent estimation results in two temporal lobe epilepsy patients. Right panel of Fig. 6.7 shows the quantitative results in the five studied patients by comparing with the iEEG-SOZ and surgical resection. Fig. 6.7(a) shows the results in a left temporal epilepsy patient and the results were compared with the iEEG-SOZ of the patient. Fig. 6.7(b) shows the result in a right temporal epilepsy patient and the results were compared with the surgical resection of the patient. It can be seen from the quantitative results of the Fig 7(c) that there are about 50% and 90% overlapping with the source solution and the SOZ respectively, when the SOZ of intracranial recording

were compared. There are about 70% overlapping with the source solution and resected region, when the surgical resections of the patients were compared.

6.4 Discussion

When studying the interictal spikes of a patient with focal partial epilepsy, the epileptogenic zone responsible for generating spikes is located in a focal area; thus, the distribution of the current source of this activity can be assumed to be active, i.e. nonzero, in a continuous area and non-active in other areas. In sparse processing language, this characteristic of source distribution translates to sparse edges. Taking the gradient of the spatial current distribution will result in a sparse signal, as only the boundary of the source has the nonzero spatial gradient of the sources. This prior knowledge can be incorporated in the problem to achieve better results. This new proposed method can potentially yield better results as it is using a priori information which was not directly incorporated in previous inverse methods. Although, previous methods such as LORETA tried to impose a smoothness condition by including an additional regularization term containing the Laplacian of the current distribution, yet the outcome was pretty smoothed as the L2 norm was used in that case. By performing the sparse L1 norm on the spatial gradient of the source, we are able to reconstruct the signal that only has limited spatial jump, i.e. the edges of the source distribution.

In order to reach better inverse solutions any sort of redundancy in the underlying process of the problem, i.e. generation of spikes in brain tissue, should be used to better use the limited scalp measurements. This means that using powerful data analysis tools

such as sparse signal processing techniques will remedy the problem, due to the fact that in many natural phenomena there is some sort of redundancy in the underlying process which if properly understood and studied could potentially be used to extract more information and thus solve the problem more efficiently. This means that taking the right mathematical transform from a seemingly non-sparse signal can project the signal into a sparse domain, i.e. more data elements being zero. This translates to a smaller number of variables, which implies that the limited number of measurements can be used to solve the underdetermined problem, more effectively. As an example, a piecewise continuous signal is not sparse as it has many non-zero elements, but when the spatial derivative of this signal is taken, only the edges will remain non-zero. Thus an inherently non-sparse signal can be transformed into a domain where it is sparse and has more zero elements.

The solution to equation (6.3) is generally a better solution than the weighted minimum norm like solutions, in the sense that the solution is limited in space (without any subjective thresholding); however, it still depends on the hyper-parameter λ. If λ is too small, the solution will be noisy and unstable, i.e. there will be alternating non-zero current dipoles in the originally silent background. On the other hand if λ is large, the solution is smooth but overestimating the extent quite extensively (specifically in the case of small simulated sources). As a result, the optimization problem in (6.3) is a good step towards a better solution, yet does not meet the set goals. We propose a multi-resolution method to accurately estimate the source extent in a two-step approach as shown in equation (6.4). The edge sparse estimation method together with the multi-resolution method is a good strategy for solving the regularized inverse problem with great accuracy.

In conclusion, we proposed an approach for imaging the source extent from noninvasive EEG. The edge sparse method and multi-resolution method were utilized to accurately estimate the source extent. The approach was studied in a series of computer simulations and patient data analysis, and the results are consistent with the simulated source size and the clinically diagnosed epileptic source size. The study demonstrates the usefulness of utilizing sparse method in estimating the source extent and it indicates the potential application of identifying both the source location and source extent for the epileptic activity.

Chapter 7 Summary and Conclusions

Functional neuroimaging is a great tool to study the underlying brain source from noninvasive scalp EEG. It is of enormous importance to study the normal brain function and pathological diseased brain. In this dissertation, we intensively studied the feasibility of utilizing the EEG source image approaches to noninvasively imaging the epileptic sources. Both the source-space connectivity method and dynamic seizure imaging approaches have shown promise in localizing and tracking the seizure activities. The EEG source imaging can help to noninvasively image the scalp recorded high-frequency activity to better study the pathological biomarker of epileptogenesis. Our study also demonstrates the potential application of spare method in estimating the source extent, which will enable us to estimate both the location and extent of the epileptogenic zone. In overall, the present study demonstrates the feasibility of high-density EEG recordings and high-resolution EEG source imaging in localizing epileptic activities and indicates its potential usage in pre-surgical planning of epilepsy patients.

Despite the development and clinical application of various imaging techniques, accurately localizing epileptogenic zones in pre-surgical workup of medically intractable epilepsy remains to be vitally important. Intracranial recordings utilizing subdural grids and depth electrodes are currently the gold standards of identifying the position and extent of epileptogenic zones. Due to the limited spatial coverage and invasive nature of intracranial grids, many noninvasive functional neuroimaging techniques (PET, SPECT, fMRI) have been developed to enhance pre-surgical planning. Each of these functional

neuroimaging techniques enables the capture of additional useful information for pre-surgical workup and, ultimately, enhanced outcomes of epilepsy patients. However, these extant techniques have poor temporal resolution and may not indicate the precise epileptogenic zone, but rather regions of seizure propagation. On the other hand, EEG represents a direct measurement of brain electrophysiological activities and has a high temporal resolution (at millisecond scale), which makes it possible to study the initiation and propagation of epileptiform discharges and seizure activities. Long-term video EEG monitoring is now available as a routine procedure in most clinical centers, and could be a more useful pre-surgical evaluation tool when coupled with source analysis techniques.

Due to the availability and feasibility of dense array EEG recording systems, high-density EEG source imaging has been attracting more and more attention from epilepsy researchers and clinicians. Studies have shown that more recording electrodes allow for accurate epileptic source localization results (Lantz, et al., 2003). A great precision in localizing interictal epileptic activity was reported by applying high-density EEG source imaging in epilepsy patients (Michel et al., 2004). In contrast to routine scalp EEG recordings in current clinical settings, which only use 19-21 recording electrodes, in this study we utilized high-density EEG with 76 channels to localize ictal onset zones with high resolution. We also compared the source imaging results in different electrode configurations by downsampling 76 channels into 64, 48, 32, and 21 channels. Our results demonstrated the significant improvement of EEG source localization by increasing the electrode numbers. That is, the most significantly improved result was observed in configurations with 76 electrodes. The potential application of high-density

EEG may provide more information than the traditional scalp EEG recordings and help lateralizing or localizing epileptogenic zones.

An important issue in EEG source imaging is modeling source configurations and choosing inverse algorithms. Dipolar source model and distributed source model are the most commonly used source models in EEG source imaging (He et al, 2002; Michel et al., 2004). The assumption for dipolar source model is that a few discrete sources are adequate to explain the scalp potential. Studies have shown that equivalent current dipolar source model can be successfully applied in localizing focal epileptiform activities (Assaf and Ebersole, 1997; Gavarat et al., 2004). However, *a priori* knowledge of the source number is usually hard to determine and dipolar models cannot adequately represent the extent of the sources, despite efforts on estimation of the number of dipoles (Bai and He, 2005, 2006). In distributed source models, current sources are located in the whole source space such as 3D brain volume or 2D cortical surface. Various inverse methods were successfully employed to image the electrical sources of epilepsy patients (Assaf and Ebersole, 1997; Gavarat et al., 2004; Michel et al., 2004; Holmes, 2008). To utilize EEG source analysis as a pre-surgical evaluation tool in clinical procedure, more studies are needed to investigate the feasibility of source imaging approaches in localizing epileptogenic foci of epilepsy patients.

Another challenging problem in pre-surgical planning of epilepsy patients is to identify the epileptogenic zones in MRI-negative patients. With the advancement of MRI imaging techniques, more mild changes in brain structure could now be visible in MRI scans. However, it is not rare to have epilepsy patients with normal images in various

MRI scan sequences (Rosenow and Lüders, 2001; Brodbeck et al., 2010). Furthermore, the structural lesions visible in MRI may not be epileptic and the true epileptic brain tissue may exist in regions that are distinct from the MRI lesions. Noninvasive approaches localizing epileptic regions are thus extremely helpful in these MRI-negative patients. More studies are still needed to further investigate the additional value of noninvasive EEG in MRI-negative patients, which will help to test the feasibility of functional neuroimaging in localizing epileptic regions with normal MRI.

Reference

Akiyama T, Chan DW, Go CY, Ochi A, Elliott IM, Donner EJ, et al. Topographic movie of intracranial ictal high-frequency oscillations with seizure semiology: Epileptic network in Jacksonian seizures. Epilepsia 2011;52:75-83.

Andrade-Valenca L, Dubeau F, Mari F, Zelmann R, Gotman J. Interictal scalp fast oscillations as a marker of the seizure onset zone. Neurology 2011;77:524-531.

Assaf BA, Ebersole JS. Continuous source imaging of scalp ictal rhythms in temporal lobe epilepsy. Epilepsia 1997;38:1114-1123.

Astolfi L, Cincotti F, Babiloni C, Carducci F, Basilisco A, Rossini PM, et al. Estimation of the cortical connectivity by high-resolution EEG and structural equation modeling: simulations and application to finger tapping data. IEEE Trans. Biomed. Eng. 2005;52:757-768.

Astolfi L, Cincotti F, Mattia D, Salinari S, Babiloni C, Basilisco A, et al. Estimation of the effective and functional human cortical connectivity with structural equation modeling and directed transfer function applied to high-resolution EEG. Magn.Reson.Imaging 2004;22:1457-1470.

Ayala M, Cabrerizo M, Jayakar P, Adjouadi M. Subdural EEG Classification Into Seizure and Nonseizure Files Using Neural Networks in the Gamma Frequency Band. J. Clin. Neurophysiol. 2011;28:20.

Babiloni F, Cincotti F, Babiloni C, Carducci F, Mattia D, Astolfi L, et al. Estimation of the cortical functional connectivity with the multimodal integration of high-resolution EEG and fMRI data by directed transfer function. Neuroimage 2005;24:118-131.

Bai X, He B. Estimation of number of independent brain electric sources from the scalp EEGs. IEEE Trans. Biomed. Eng. 2006;53:1883-1892.

Bai X, He B. On the estimation of the number of dipole sources in EEG source localization. Clin. Neurophysiol. 2005;116:2037-2043.

Baillet S, Mosher JC, Leahy RM. Electromagnetic brain mapping. Signal Processing Magazine, IEEE 2001;18:14-30.

Billings S, Zhao Y, Wei H, Sarrigiannis PG. A parametric method to measure time-varying linear and nonlinear causality with Applications to EEG data. IEEE Trans. Biomed. Eng. 2013;60:3141-3148.

Boon P, D'Havé M, Vanrumste B, Van Hoey G, Vonck K, Van Walleghem P, et al. Ictal source localization in presurgical patients with refractory epilepsy. J. Clin. Neurophysiol. 2002;19:461-468.

Bragin A, Engel J, Wilson CL, Fried I, Buzsáki G. High-frequency oscillations in human brain. Hippocampus 1999;9:137-142.

Brodbeck V, Lascano AM, Spinelli L, Seeck M, Michel CM. Accuracy of EEG source imaging of epileptic spikes in patients with large brain lesions. Clin. Neurophysiol. 2009;120:679-685.

Brodbeck V, Spinelli L, Lascano AM, Pollo C, Schaller K, Vargas MI, et al. Electrical source imaging for presurgical focus localization in epilepsy patients with normal MRI. Epilepsia 2010;51:583-591.

Cascino GD. Commentary: how has neuroimaging improved patient care? Epilepsia 1994;35:S103-S107.

Crépon B, Navarro V, Hasboun D, Clemenceau S, Martinerie J, Baulac M, et al. Mapping interictal oscillations greater than 200 Hz recorded with intracranial macroelectrodes in human epilepsy. Brain 2010;133:33-45.

Dale AM, Liu AK, Fischl BR, Buckner RL, Belliveau JW, Lewine JD, et al. Dynamic Statistical Parametric Mapping: Combining fMRI and MEG for High-Resolution Imaging of Cortical Activity. Neuron 2000;26:55-67.

Dale AM, Sereno MI. Improved localizadon of cortical activity by combining eeg and meg with mri cortical surface reconstruction: A linear approach. J. Cogn. Neurosci. 1993;5:162-176.

Darvas F, Pantazis D, Kucukaltun-Yildirim E, Leahy RM. Mapping human brain function with MEG and EEG: methods and validation. Neuroimage 2004;23:S289-S299.

Delorme A, Makeig S. EEGLAB: an open source toolbox for analysis of single-trial EEG dynamics including independent component analysis. J.Neurosci.Methods 2004;134:9-21.

Ding L, He B. Spatio-temporal EEG source localization using a three-dimensional subspace FINE approach in a realistic geometry inhomogeneous head model. IEEE Trans. Biomed. Eng. 2006;53:1732-1739.

Ding L, Worrell GA, Lagerlund TD, He B. Ictal source analysis: localization and imaging of causal interactions in humans. Neuroimage 2007;34:575-586.

Ebersole JS. Noninvasive localization of epileptogenic foci by EEG source modeling. Epilepsia 2000;41:S24-S33.

Ebersole JS, Hawes-Ebersole S. Clinical application of dipole models in the localization of epileptiform activity. Journal of Clinical Neurophysiology 2007;24:120-129.

Engel Jr J. Surgical treatment for epilepsy: too little, too late? JAMA 2008;300:2548-2550.

Engel Jr J. Approaches to localization of the epileptogenic lesion. In: Engel Jr J, editor. Surgical treatment of the epilepsies. New York: Raven Press, 1987: 75-95.

Engel Jr. J, da Silva FL. High-frequency oscillations – Where we are and where we need to go. Prog.Neurobiol. 2012;98:316-318.

Fisher RS, van Emde Boas W, Blume W, Elger C, Genton P, Lee P, et al. Epileptic seizures and epilepsy: definitions proposed by the International League Against Epilepsy (ILAE) and the International Bureau for Epilepsy (IBE). Epilepsia 2005;46:470-472.

Fisher RS, Vickrey BG, Gibson P, Hermann B, Penovich P, Scherer A, et al. The impact of epilepsy from the patient's perspective I. Descriptions and subjective perceptions. Epilepsy Res. 2000;41:39-51.

Gavaret M, Badier JM, Marquis P, Bartolomei F, Chauvel P. Electric source imaging in temporal lobe epilepsy. J. Clin. Neurophysiol. 2004;21:267-282.

Gavaret M, Badier JM, Marquis P, McGonigal A, Bartolomei F, Regis J, et al. Electric source imaging in frontal lobe epilepsy. J. Clin. Neurophysiol. 2006;23:358-370.

Gilliam F, Wyllie E, Kashden J, Faught E, Kotagal P, Bebin M, et al. Epilepsy surgery outcome: comprehensive assessment in children. Neurology 1997;48:1368.

Gotman J. Epileptic networks studied with EEG-fMRI. Epilepsia 2008;49:42-51.

Gotman J, Kobayashi E, Bagshaw AP, Bénar CG, Dubeau F. Combining EEG and fMRI: a multimodal tool for epilepsy research. J. Magn. Reson. Imaging 2006;23:906-920.

Granger CWJ. Investigating causal relations by econometric models and cross-spectral methods. Econometrica 1969;37:424-438.

Guggisberg AG, Kirsch HE, Mantle MM, Barbaro NM, Nagarajan SS. Fast oscillations associated with interictal spikes localize the epileptogenic zone in patients with partial epilepsy. Neuroimage 2008;39:661-668.

Hämäläinen MS, Ilmoniemi RJ. Interpreting measured magnetic fields of the brain: estimates of current distributions. Helsinki Univ.Technol., Helsinki, Finland, Tech.Rep.TKK-F- A 1984.

Hämäläinen MS, Sarvas J. Realistic conductivity geometry model of the human head for interpretation of neuromagnetic data. IEEE Trans. Biomed. Eng. 1989;36:165-171.

He B. Neural engineering. 2nd ed. New York: Springer, 2013.

He B, Liu Z. Multimodal functional neuroimaging: Integrating functional MRI and EEG/MEG. IEEE Rev. Biomed. Eng. 2008;1:23-40.

He B, Musha T, Okamoto Y, Homma S, Nakajima Y, Sato T. Electric dipole tracing in the brain by means of the boundary element method and its accuracy. IEEE Trans. Biomed. Eng. 1987;34:406-414.

He B, Yang L, Wilke C, Yuan H. Electrophysiological Imaging of Brain Activity and Connectivity – Challenges and Opportunities. IEEE Trans. Biomed. Eng. 2011;58:1918-31.

He B, Zhang X, Lian J, Sasaki H, Wu D, Towle VL. Boundary element method-based cortical potential imaging of somatosensory evoked potentials using subjects' magnetic resonance images. Neuroimage 2002;16:564-576.

He B, Dai Y, Astolfi L, Babiloni F, Yuan H, Yang L. < i> eConnectome</i>: A MATLAB toolbox for mapping and imaging of brain functional connectivity. J.Neurosci.Methods 2011;195:261-269.

He B, Ding L. Electrophysiological Mapping and Neuroimaging. In: He B, editor. Neural Engineering. New York: Springer, 2013: 499-543.

Herrendorf G, Steinhoff B, Kolle R, Baudewig J, Waberski T, Buchner H, et al. Dipole-Source Analysis in a Realistic Head Model in Patients with Focal Epilepsy. Epilepsia 2000;41:71-80.

Holmes MD. Dense array EEG: Methodology and new hypothesis on epilepsy syndromes. Epilepsia 2008;49:3-14.

Holmes MD, Tucker DM, Quiring JM, Hakimian S, Miller JW, Ojemann JG. Comparing Noninvasive Dense Array and Intracranial Electroencephalography for Localization of Seizures. Neurosurgery 2010;66:354-362.

Jacobs J, LeVan P, Chander R, Hall J, Dubeau F, Gotman J. Interictal high-frequency oscillations (80–500 Hz) are an indicator of seizure onset areas independent of spikes in the human epileptic brain. Epilepsia 2008;49:1893-1907.

Jacobs J, LeVan P, Châtillon C, Olivier A, Dubeau F, Gotman J. High frequency oscillations in intracranial EEGs mark epileptogenicity rather than lesion type. Brain 2009;132:1022-1037.

Jacobs J, Zijlmans M, Zelmann R, Chatillon C, Hall J, Olivier A, et al. High-frequency electroencephalographic oscillations correlate with outcome of epilepsy surgery. Ann.Neurol. 2010;67:209-220.

Jacobs J, Staba R, Asano E, Otsubo H, Wu JY, Zijlmans M, et al. High-frequency oscillations (HFOs) in clinical epilepsy. Prog.Neurobiol. 2012;98:302-315.

Jirsch J, Urrestarazu E, LeVan P, Olivier A, Dubeau F, Gotman J. High-frequency oscillations during human focal seizures. Brain 2006;129:1593-1608.

Jung KY, Kang JK, Kim JH, Im CH, Kim KH, Jung HK. Spatiotemporospectral characteristics of scalp ictal EEG in mesial temporal lobe epilepsy with hippocampal sclerosis. Brain Res. 2009;1287:206-219.

Jung TP, Makeig S, Humphries C, Lee TW, Mckeown MJ, Iragui V, et al. Removing electroencephalographic artifacts by blind source separation. Psychophysiology 2000;37:163-178.

Kaiboriboon K, Nagarajan S, Mantle M, Kirsch HE. Interictal MEG/MSI in intractable mesial temporal lobe epilepsy: spike yield and characterization. Clinical Neurophysiology 2010;121:325-331.

Kamiński M, Ding M, Truccolo WA, Bressler SL. Evaluating causal relations in neural systems: Granger causality, directed transfer function and statistical assessment of significance. Biol.Cybern. 2001;85:145-157.

Kaminski MJ, Blinowska KJ. A new method of the description of the information flow in the brain structures. Biol.Cybern. 1991;65:203-210.

Kobayashi K, Yoshinaga H, Toda Y, Inoue T, Oka M, Ohtsuka Y. High-frequency oscillations in idiopathic partial epilepsy of childhood. Epilepsia 2011;52:1812-1819.

Koessler L, Benar C, Maillard L, Badier JM, Vignal JP, Bartolomei F, et al. Source localization of ictal epileptic activity investigated by high resolution EEG and validated by SEEG. Neuroimage 2010;51:642-653.

Lachaux J, Fonlupt P, Kahane P, Minotti L, Hoffmann D, Bertrand O, et al. Relationship between task-related gamma oscillations and BOLD signal: New insights from combined fMRI and intracranial EEG. Hum.Brain Mapp. 2007;28:1368-1375.

Lai Y, Van Drongelen W, Ding L, Hecox K, Towle V, Frim D, et al. Estimation of in vivo human brain-to-skull conductivity ratio from simultaneous extra-and intra-cranial electrical potential recordings. Clin. Neurophysiol. 2005;116:456-465.

Lai Y, van Drongelen W, Hecox K, Frim D, Kohrman M, He B. Cortical activation mapping of epileptiform activity derived from interictal ECoG spikes. Epilepsia 2007;48:305-314.

Lai Y, Zhang X, van Drongelen W, Korhman M, Hecox K, Ni Y, et al. Noninvasive cortical imaging of epileptiform activities from interictal spikes in pediatric patients. Neuroimage 2011;54:244-252.

Lantz G, Grave de Peralta R, Spinelli L, Seeck M, Michel CM. Epileptic source localization with high density EEG: how many electrodes are needed? Clin. Neurophysiol. 2003;114:63-69.

Lantz G, Michel CM, Seeck M, Blanke O, Spinelli L, Thut G, et al. Space-oriented segmentation and 3-dimensional source reconstruction of ictal EEG patterns. Clin. Neurophysiol. 2001;112:688-697.

Leahy R, Mosher J, Spencer M, Huang M, Lewine J. A study of dipole localization accuracy for MEG and EEG using a human skull phantom. Electroencephalogr.Clin.Neurophysiol. 1998;107:159-173.

Liu Z, He B. fMRI-EEG integrated cortical source imaging by use of time-variant spatial constraints. Neuroimage 2008;39:1198-1214.

Lu Y, Yang L, Worrell GA, He B. Seizure source imaging by means of FINE spatio-temporal dipole localization and directed transfer function in partial epilepsy patients. Clinical Neurophysiology 2012a;123:1275-1283.

Lu Y, Yang L, Worrell GA, Brinkmann B, Nelson C, He B. Dynamic imaging of seizure activity in pediatric epilepsy patients. Clin. Neurophysiol. 2012b;123:2122-2129.

Lu Y, Worrell G, Zhang H, Yang L, Brinkmann B, Nelson C, et al. Noninvasive Imaging of the High Frequency Brain Activity in Focal Epilepsy Patients. IEEE Trans. Biomed. Eng. 2014;61:1660-1667.

Malmivuo J, Plonsey R. Bioelectromagnetism: principles and applications of bioelectric and biomagnetic fields. : Oxford University Press, 1995.

Merlet I, Gotman J. Dipole modeling of scalp electroencephalogram epileptic discharges: correlation with intracerebral fields. Clin. Neurophysiol. 2001;112:414-430.

Michel CM, Lantz G, Spinelli L, de Peralta RG, Landis T, Seeck M. 128-channel EEG source imaging in epilepsy: clinical yield and localization precision. J. Clin. Neurophysiol. 2004;21:71-83.

Michel CM, Murray MM, Lantz G, Gonzalez S, Spinelli L, Grave de Peralta R. EEG source imaging. Clin. Neurophysiol. 2004;115:2195-2222.

Moeller F, LeVan P, Gotman J. Independent component analysis (ICA) of generalized spike wave discharges in fMRI: Comparison with general linear model-based EEG-fMRI. Hum.Brain Mapp. 2011;32:209-217.

Morrell MJ. Responsive cortical stimulation for the treatment of medically intractable partial epilepsy. Neurology 2011;77:1295-1304.

Mosher JC, Leahy RM. Source localization using recursively applied and projected (RAP) MUSIC. IEEE Trans. Signal Proc. 1999;47:332-340.

Nam H, Yim TG, Han SK, Oh JB, Lee SK. Independent component analysis of ictal EEG in medial temporal lobe epilepsy. Epilepsia 2002;43:160-164.

Ochi A, Otsubo H, Donner EJ, Elliott I, Iwata R, Funaki T, et al. Dynamic Changes of Ictal High-Frequency Oscillations in Neocortical Epilepsy: Using Multiple Band Frequency Analysis. Epilepsia 2007;48:286-296.

Oishi M, Otsubo H, Kameyama S, Morota N, Masuda H, Kitayama M, et al. Epileptic spikes: magnetoencephalography versus simultaneous electrocorticography. Epilepsia 2002;43:1390-1395.

Oostendorp TF, Delbeke J, Stegeman DF. The conductivity of the human skull: results of in vivo and in vitro measurements. IEEE Trans. Biomed. Eng. 2000;47:1487-1492.

Palmini A, Andermann F, Olivier A, Tampieri D, Robitaille Y. Focal neuronal migration disorders and intractable partial epilepsy: results of surgical treatment. Ann.Neurol. 1991;30:750-757.

Pascual-Marqui RD. Standardized low-resolution brain electromagnetic tomography (sLORETA): technical details. Methods Find. Exp. Clin. Pharmacol. 2002;24:5-12.

Patel A, Alotaibi F, Blume WT, Mirsattari SM. Independent component analysis of subdurally recorded occipital seizures. Clin. Neurophysiol. 2008;119:2437-2446.

Pittau F, LeVan P, Moeller F, Gholipour T, Haegelen C, Zelmann R, et al. Changes preceding interictal epileptic EEG abnormalities: Comparison between EEG/fMRI and intracerebral EEG. Epilepsia 2011;52:1120-1129.

Plummer C, Harvey AS, Cook M. EEG source localization in focal epilepsy: Where are we now? Epilepsia 2008;49:201-218.

Plummer C, Litewka L, Farish S, Harvey A, Cook M. Clinical utility of current-generation dipole modelling of scalp EEG. Clinical Neurophysiology 2007;118:2344-2361.

Rosenow F, Lüders H. Presurgical evaluation of epilepsy. Brain 2001;124:1683.

Sekihara K, Nagarajan SS, Poeppel D, Marantz A, Miyashita Y. Reconstructing spatio-temporal activities of neural sources using an MEG vector beamformer technique. IEEE Trans. Biomed. Eng. 2001;48:760-771.

Shinnar S, Pellock JM. Update on the epidemiology and prognosis of pediatric epilepsy. J.Child Neurol. 2002;17:S4.

Siegel AM, Cascino GD, Meyer FB, McClelland RL, So EL, Marsh WR, et al. Resective reoperation for failed epilepsy surgery: seizure outcome in 64 patients. Neurology 2004;63:2298-2302.

Sperli F, Spinelli L, Seeck M, Kurian M, Michel CM, Lantz G. EEG source imaging in pediatric epilepsy surgery: a new perspective in presurgical workup. Epilepsia 2006;47:981-990.

Staba RJ, Frighetto L, Behnke EJ, Mathern GW, Fields T, Bragin A, et al. Increased fast ripple to ripple ratios correlate with reduced hippocampal volumes and neuron loss in temporal lobe epilepsy patients. Epilepsia 2007;48:2130-2138.

Tito M, Cabrerizo M, Ayala M, Jayakar P, Adjouadi M. A comparative study of intracranial EEG files using nonlinear classification methods. Ann.Biomed.Eng. 2010;38:187-199.

Tito M, Cabrerizo M, Ayala M, Jayakar P, Adjouadi M. Seizure detection: an assessment of time-and frequency-based features in a unified two-dimensional decisional space using nonlinear decision functions. Journal of Clinical Neurophysiology 2009;26:381.

Van Paesschen W, Dupont P, Sunaert S, Goffin K, Van Laere K. The use of SPECT and PET in routine clinical practice in epilepsy. Curr.Opin.Neurol. 2007;20:194-202.

Van Veen BD, Van Drongelen W, Yuchtman M, Suzuki A. Localization of brain electrical activity via linearly constrained minimum variance spatial filtering. IEEE Trans. Biomed. Eng. 1997;44:867-880.

Vulliemoz S, Carmichael DW, Rosenkranz K, Diehl B, Rodionov R, Walker MC, et al. Simultaneous intracranial EEG and fMRI of interictal epileptic discharges in humans. Neuroimage 2011;54:182-190.

Wagner M, Fuchs M, Kastner J. SWARM: sLORETA-weighted accurate minimum norm inverse solutions. International Congress Series 2007;1300:185-188.

Wang G, Worrell G, Yang L, Wilke C, He B. Interictal spike analysis of high-density EEG in patients with partial epilepsy. Clin. Neurophysiol. 2010;122:1098-1105.

Wang ZI, Jin K, Kakisaka Y, Mosher JC, Bingaman WE, Kotagal P, et al. Imag (in) ing seizure propagation: MEG-guided interpretation of epileptic activity from a deep source. Hum.Brain Mapp. 2012.

Wilke C, Van Drongelen W, Kohrman M, He B. Neocortical seizure foci localization by means of a directed transfer function method. Epilepsia 2010;51:564-572.

Wilke C, Van Drongelen W, Kohrman M, He B. Identification of epileptogenic foci from causal analysis of ECoG interictal spike activity. Clin. Neurophysiol. 2009;120:1449-1456.

Wilke C, Worrell G, He B. Graph analysis of epileptogenic networks in human partial epilepsy. Epilepsia 2011;52:84-93.

Worrell GA, Lagerlund TD, Sharbrough FW, Brinkmann BH, Busacker NE, Cicora KM, et al. Localization of the epileptic focus by low-resolution electromagnetic tomography in patients with a lesion demonstrated by MRI. Brain Topogr. 2000;12:273-282.

Worrell GA, Gardner AB, Stead SM, Hu S, Goerss S, Cascino GJ, et al. High-frequency oscillations in human temporal lobe: simultaneous microwire and clinical macroelectrode recordings. Brain 2008;131:928-937.

Worrell G, Gotman J. High-frequency oscillations and other electrophysiological biomarkers of epilepsy: clinical studies. Biomarkers 2011;5:557-566.

Worrell GA, Jerbi K, Kobayashi K, Lina JM, Zelmann R, Le Van Quyen M. Recording and analysis techniques for high-frequency oscillations. Prog.Neurobiol. 2012;98:265-278.

Wu J, Sankar R, Lerner J, Matsumoto J, Vinters H, Mathern G. Removing interictal fast ripples on electrocorticography linked with seizure freedom in children. Neurology 2010;75:1686-1694.

Xu XL, Xu B, He B. An alternative subspace approach to EEG dipole source localization. Phys.Med.Biol. 2004;49:327.

Yang L, Liu Z, He B. EEG-fMRI reciprocal functional neuroimaging. Clin. Neurophysiol. 2010;121:1240-1250.

Yang L, Wilke C, Brinkmann B, Worrell GA, He B. Dynamic imaging of ictal oscillations using non-invasive high-resolution EEG. Neuroimage 2011;56:1908-1917.

Yang L, Worrell GA, Nelson C, Brinkmann B, He B. Spectral and spatial shifts of post-ictal slow waves in temporal lobe seizures. Brain 2012;135:3134-3143.

You X, Adjouadi M, Guillen MR, Ayala M, Barreto A, Rishe N, et al. Sub-patterns of language network reorganization in pediatric localization related epilepsy: A multisite study. Hum.Brain Mapp. 2011;32:784-799.

Zhang X, van Drongelen W, Hecox KE, Towle VL, Frim DM, McGee AB, et al. High-resolution EEG: Cortical potential imaging of interictal spikes. Clin. Neurophysiol. 2003;114:1963-1973.

Zhang Y, van Drongelen W, He B. Estimation of in vivo brain-to-skull conductivity ratio in humans. Appl.Phys.Lett. 2006;89:223903.

Publication List

Peer-reviewed journal articles

1. **Y. Lu**, G. Worrell, H.C. Zhang, L. Yang, B. Brinkmann, C. Nelson, B. He. "Noninvasive Imaging of the High Frequency Brain Activity in Focal Epilepsy Patients", *IEEE Transactions on Biomedical Engineering*, Vol. 61(6), pp. 1660–1667, 2014.

2. **Y. Lu**, L. Yang, G. Worrell, B. Brinkmann, C. Nelson, B. He. "Dynamic imaging of seizure activity in pediatric epilepsy patients", *Clinical Neurophysiology*, Vol. 123(11), pp. 2122–2129, 2012. **(Journal Cover Article)**

3. **Y. Lu**, L. Yang, G. Worrell, B. He. "Seizure source imaging by means of FINE spatio-temporal dipole localization and directed transfer function in partial epilepsy patients", *Clinical Neurophysiology,* vol. 123(7), 1275-83, 2012.

4. H. Xu, **Y. Lu**, S. Zhu, B. He. "Assessing Dynamic Spectral Causality by Lagged Adaptive Directed Transfer Function and Instantaneous Effect Factor", *IEEE Transactions on Biomedical Engineering*, doi: 10.1109/TBME.2014.2311034, 2014.

5. C. Zhang, **Y. Lu**, B. Brinkmann, K. Welker, G. Worrell, Bin He. "Lateralization and Localization of Epilepsy Related Hemodynamic Foci Using Presurgical fMRI", *Clinical Neurophysiology,* in press, 2014.

6. A. Sohrabpour, **Y. Lu**, P. Kankirawatana, J. Blount, H. Kim, B. He. "Effect of EEG Electrode Number on Epileptic Source Localization in Pediatric Patients" *Clinical Neurophysiology,* in press, 2014.

Conference proceeding publications

1. **Y. Lu**, G. Worrell, C. Zhang, A. Sohrabpour, B. He. "EEG Source Imaging and Connectivity Analysis in Epilepsy Patients", *Proc. of Annual Asilomar Conf. on Signals, Systems, and Computers,* 2013.

2. **Y. Lu**, L. Yang, G. Worrell, B. Brinkmann, C. Nelson, B. He. "Dynamic seizure imaging in patients with extratemporal lobe epilepsy ", *Proc. of Annual Int'l Conf. of IEEE-EMBS,* pp. 6228-6231, 2012. **(Student Paper Competition Award)**

3. Sohrabpour, **Y. Lu**, P. Kankirawatana, B. He. "EEG Electrode Configuration and Source Imaging." *Journal of Medical Devices*, doi:10.1115/1.4027019, 2014.

4. Zhang, **Y. Lu**, B. He. "Sustained Thermal Pain Modulates Spontaneous Sensorimotor Rhythms", *Proc. of Annual Int'l Conf. of IEEE-EMBS on Neural Engineering*, pp. 759-760, 2013.

5. Kober, C. Landes, A. Preiss, **Y. Lu**, P. Young, R. Sader, "Computer Aided Monitoring of Bone Quality and New Bone Formation upon Distractive Maxillary Expansion based on Pre- and Post-Surgical CT-Data", *Proc. of 4th European Conf. of International Federation for Medical and Biological Engineering,* vol. 22, pp. 530–532, 2009.

Conference presentations/abstracts

1. **Y. Lu**, H. Zhang, et al., "Localization of epileptogenic brain from high density scalp EEG and fMRI", *Int'l conf. on Basic and Clinical multimodal Imaging,* Geveva, Switzerland, 2013

2. **Y. Lu**, H. Zhang, G. Worrell, et al. "Mapping the High Frequency Epileptic Brain Activity from Scalp EEG", *19th Annual Meeting Organization for Human Brain Mapping*, Seattle, WA, 2013.

3. **Y. Lu**, L. Yang, et al., "Dynamic imaging of seizure activity using non-invasive high-resolution EEG", *Curing the Epilepsies 2013: Pathways Forward Conference*, National Institute of Neurological Disorders and Stroke (NINDS), NIH, Washington D.C., 2013. **(Travel Award)**

4. **Y. Lu**, H. Zhang, G. Worrell, et al. "Noninvasive Mapping of the High Frequency Brain Activity in Focal Epilepsy Patients", *67th Annual Meeting American Epilepsy Society*, Washington, D.C., 2013.

5. **Y. Lu**, L. Yang, B. Brinkmann, et al., "Dynamic seizure imaging in pediatric patients with partial epilepsy", *66th Annual Meeting American Epilepsy Society*, San Diego, CA, 2012.

6. **Y. Lu**, P. Kankirawatana, L. Yang, H. Kim, J. Blount, B. He, "Seizure Source Imaging in Pediatric Patients using Dense Array EEG", *65th Annual Meeting American Epilepsy Society*, Baltimore, MD, 2011.

7. **Y. Lu**, L. Yang, G. Worrell, B. He, “High-density EEG Source Imaging and Connectivity Analysis in Partial Epilepsy Patients”, *64th Annual Meeting American Epilepsy Society*, San Antonio, TX, 2010.